ABSTRACT

Guo, Weijun. **Improving the MCLLS Method Applied to the *In Vivo* XRF Measurement of Lead in Bone by Using the Differential Operator Approach (MCDOLLS) and X-ray Coincidence Spectroscopy**. (Under the direction of Prof. Robin P. Gardner).

Lead is a toxic chemical element with irreversible neurological effects on human being, which accumulates in human bones after ingestion or inhalation. To make *in vivo* measurement of the lead concentration in human bones, the Monte Carlo – Library Least-Squares (MCLLS) method has been applied with an energy-dispersive X-ray fluorescence (EDXRF) Germanium spectrometer. The quantitative result is accurate compared to the certified lead concentration of the bone sample for measurement.

To quantitatively study the matrix effect for EDXRF measurement and the measurement sensitivity, the Monte Carlo - Differential Operator method has been implemented to simulate differential responses of sample and elemental library spectra to variations of elemental compositions.

The MCLLS method requires initial guesses for elemental compositions of the sample, which causes possibly several iterations of the Monte Carlo simulation code. To improve the efficiency of the MCLLS method, a combined method (MCDOLLS) has been implemented by using Taylor series expansion to re-adjust those elemental library spectra instead of

running the simulation code one more time. Simulation cases of MCDOLLS show promising results for the *in vivo* lead in bone measurement. This method is generally applicable to other EDXRF applications with further investigation and benchmark.

Source photons back-scattered from the sample are the dominant background for *in vivo* lead in bone measurement that prevents the improvement of measurement sensitivity. X-ray coincidence spectroscopy has been investigated in this thesis to minimize the detection of events that are not correlated in time, in other word, to relatively enhance the measurement sensitivity of K and L X rays of lead, which are in true coincidence theoretically. Coincidence experiments show good results to support the theory and Monte Carlo simulation results have been benchmarked with experimental data. For setting the electronics precisely for coincidence experiments, a complete procedure is also documented.

To apply the X-ray coincidence spectroscopy to trace level lead in bone measurement, a customized spectrometer has been proposed by combining the high efficiency and low cost feature of big X-ray NaI(Tl) detectors with the fine resolution of low energy Ge detectors. This coincidence spectrometer has been simulated with the benchmarked Monte Carlo code and preliminary results are promising.

Improving the MCLLS Method Applied to the *In Vivo* XRF Measurement of Lead in Bone by Using the Differential Operator Approach (MCDOLLS) and X-ray Coincidence Spectroscopy

by

Weijun Guo

A dissertation submitted to the Graduate Faculty of
North Carolina State University
in partial fulfillment of the
requirements for the Degree of
Doctor of Philosophy

Department of Nuclear Engineering

Raleigh, North Carolina

2003

Approved By:

Dr. Dmitriy Y. Anistratov	Dr. Matthias Stallmann
Prof. Charles W. Mayo	Prof. Robin P. Gardner, Chair

BIOGRAPHY

Weijun Guo was born in China on July 6, 1976. He is the second son of Mr. Junwen Guo and Mrs. Gai'er Gao. He spent his youth in Jingle City, Shanxi.

Weijun received his Bachelor's Degree in Engineering Physics in 1997 and his Master's Degree in Engineering Physics under the guidance of Prof. Xi'nian Zang in 1999 from Tsinghua University, China. Then he began his foreign study at North Carolina State University.

Under Prof. Gardner's advisory, the author worked on Monte Carlo simulation and nuclear instrumentation for radiation measurement applications. Along his study at NCSU, Weijun received his Master's Degree in Computer Science in 2002.

Weijun married with Yingfang Cao in 1999, his lover since college.

ACKNOWLEDGMENTS

The author would like to express his deepest appreciation to Prof. Robin P. Gardner, chairman of his Advisory Committee and Prof. Charles W. Mayo for their invaluable guidance and support throughout this work. The remaining members of his Advisory Committee, Dr. Dmitriy Y. Anistratov and Dr. Matthias Stallmann, are also highly appreciated for their comments and suggestions.

It is also gratefully appreciated for the financial support provided by the grant number 2R01ES06671 from the National Institute of Environmental Health Sciences.

Appreciation is also extended to the fine staff and faculties of the Nuclear Engineering Department. To all of his colleagues, the author would like to express his warmest thanks, with special thanks to Dr. Sanghoon Lee and Dr. Walid Metwally.

The author also would like to express his heartfelt thanks to his wife, Yingfang Cao for her love, patience, inspiration and encouragement throughout the graduate work. His parents are also highly appreciated. Without their continuous encouragement and support, he would not have achieved anything academically.

Finally, the author dedicates this dissertation to his wife, Yingfang Cao.

TABLE OF CONTENTS

LIST OF TABLES ..... **VI**

LIST OF FIGURES ..... **VII**

1. INTRODUCTION **1**

1.1. Overview 1

1.2. Review of EDXRF Analysis Methods 4

1.3. X-Ray Coincidence Spectroscopy 7

1.4. Monte Carlo Simulation Code - CEARXRF 8

2. MONTE CARLO SIMULATION CODES – CEARXRF AND CEARXRC **12**

2.1. Overview 12

2.2. Simulation Input and Output 14

2.3. General Geometry 14

2.4. Photon Transportation Model 16

2.5. CEARXRC - Monte Carlo Coincidence Simulation 18

2.6. Sampling Schemes 20

2.7. Variance Reduction Techniques 27

2.8. Experimental Benchmark 30

3. MONTE CARLO - LIBRARY LEAST-SQUARES METHOD (MCLLS) **36**

3.1. Overview 36

3.2. MCLLS Simulation Procedure and Advantages 37

3.3. Application to In Vivo Measurement of Lead in Bone 38

4. MONTE CARLO - DIFFERENTIAL OPERATOR METHOD **43**

4.1. Overview 43
4.2. Mathematical Treatment 43
4.3. Simulated Differential Responses 45

5. MCDOLLS - COMBINING THE MCLLS AND DIFFERENTIAL OPERATOR METHOD 51

5.1. Overview 51
5.2. MCDOLLS Method Procedure 52
5.3. Application to In Vivo Measurement of Lead in Bone 53

6. X-RAY COINCIDENCE SPECTROSCOPY 58

6.1. Overview 58
6.2. Timing Technology 60
6.3. Time Spectrum Measurement for Quality Assurance 64
6.4. Electronics and Setting Procedures 65
6.5. Experimental Results 67
6.6. Monte Carlo Coincidence Simulation and Benchmark Results 70
6.7. Monte Carlo Coincidence Simulation with the Proposed X-ray Coincidence Spectrometer 71
6.8. MCLLS Application to Coincidence Study for Lead Determination 72

7. CONCLUSIONS AND DISCUSSION 89

8. FUTURE WORK 92

REFERENCES 94

List of Tables

Table 2.1 Comparison table for features of CEARXRF and other general purpose Monte Carlo simulation codes 32

Table 2.2 Table for physics data library used by CEARXRF and related references 33

Table 2.3 Low energy Germanium detector characteristics pertinent to this thesis 35

Table 3.1 MCLLS quantitative results for *in vivo* lead in bone measurement by fitting the simulated sample spectrum 41

Table 3.2 MCLLS quantitative results for *in vivo* lead in bone measurement by fitting the experimental sample spectrum 41

Table 4.1 Table of equations for calculating the first-order derivative of weight correction factor to the variation of elemental compositions 47

Table 5.1 Table of elemental weight fractions of two bone samples studied for MCDOLLS simulation cases 54

Table 5.2 MCLLS quantitative results by fitting sample spectrum of case B with elemental library spectra of case A 55

Table 5.3 MCDOLLS quantitative results by fitting sample spectrum of case B with re-adjusted elemental library spectra by applying Differential Operator to those of case A 57

List of Figures

Figure 1.1 Schematics of characteristic X-ray emission and competing Auger electron process 10

Figure 1.2 Schematics of atomic shell structures and naming conventions for X-ray lines ... 10

Figure 1.3 *In Vivo* EDXRF experimental spectrum for lead in bone measurement with low energy Ge detector and Cd-109 radioisotope activation source 11

Figure 2.1 HERMETOR geometry plot of the detector-source-sample arrangement for EDXRF measurement 34

Figure 2.2 Schematics of detector-source-sample geometry for benchmarking the CEARXRF simulation applied to *in vivo* lead in bone measurement 34

Figure 2.3 CEARXRF simulated sample spectrum compared with the experimental sample spectrum 35

Figure 3.1 CEARXRF simulated sample spectrum and library spectra of lead and calcium for *in vivo* EDXRF measurement of lead in bone 40

Figure 3.2 MCLLS fitted sample spectrum compared with the experimental spectrum 42

Figure 4.1 Schematics of detector-source-sample geometry for validating CEARXRF simulated differential responses 47

Figure 4.2 Differential response of sample spectrum to the variation of Calcium composition of the sample 48

Figure 4.3 Differential response of sample spectrum to the variation of Lead composition of

the sample 48

Figure 4.4 Differential response of Calcium library spectrum to the variation of Calcium composition of the sample 49

Figure 4.5 Differential response of Calcium library spectrum to the variation of Lead composition of the sample 49

Figure 4.6 Differential response of Lead library spectrum to the variation of Calcium composition of the sample 50

Figure 4.7 Differential response of Lead library spectrum to the variation of Lead composition of the sample 50

Figure 5.1 CEARXRF simulated sample spectra for validating the MCDOLLS method 54

Figure 5.2 CEARXRF simulated sample spectrum for Case B compared with re-adjusted spectrum by applying Differential Operator to the sample spectrum of case A 55

Figure 5.3 CEARXRF simulated Calcium library spectrum for Case B compared with the re-adjusted spectrum by applying Differential Operator to the Calcium library spectrum of case A 56

Figure 5.4 CEARXRF simulated Lead library spectrum for Case B compared with the re-adjusted spectrum by applying Differential Operator to the Lead library spectrum of case A 56

Figure 6.1 Schematics of correlated and uncorrelated pulses in time 74

Figure 6.2 Schematics of $\Delta T_{delay,inherent}$, the systematic error of occurrence time measurement

for photon incidence events 74

Figure 6.3 Schematics of linearly focused photo multiplier tube structure..... 75

Figure 6.4 Electron drifting process in the Germanium crystal 75

Figure 6.5 Schematics of time jitter caused by electronic noises superimposed on incoming pulses 76

Figure 6.6 Schematics of time walk caused by pulse amplitude variation 76

Figure 6.7 Schematics of time walk caused by pulse rise time variation..... 77

Figure 6.8 Working principle of the true constant fraction (TCF) technique to pick off time 77

Figure 6.9 Working principle of the amplitude and rise time compensated (ARC) technique to pick off time 77

Figure 6.10 Schematic of electronics connection for time spectrum measurement 78

Figure 6.11 Experimental time spectrum with LEGe & X-ray NaI(Tl) detectors..... 78

Figure 6.12 Experimental time spectrum with two X-ray NaI(Tl) detectors 79

Figure 6.13 Schematics of electronics connection for two-parameter coincidence measurement 80

Figure 6.14 Screen shot of the Kamx 7 data acquisition toolsheet CEARCOINC.tlsh 81

Figure 6.15 Oscilloscope screen printout to show the timing synchronization between the coincidence gate signal and the ADC input pulse 82

Figure 6.16 Experimental singles and coincidence spectrum for pure lead measurement with two X-ray NaI(Tl) detectors..... 82

Figure 6.17 2-D scatter plot for experimental data of pure lead measurement with two X-ray NaI(Tl) detectors 83

Figure 6.18 Experimental singles and coincidence sepectra for pure lead measurement with Ge detector 83

Figure 6.19 Experimental singles and coincidence spectra for pure lead measurement with X-ray NaI(Tl) detector 84

Figure 6.20 2-D scatter plot for experimental data of pure lead measurement with NaI(Tl) detector and low energy Ge detector 84

Figure 6.21 Proposed X-ray coincidence spectrometer for *in vivo* lead in bone measurement with low energy Ge and customized X-ray NaI(Tl) detectors 85

Figure 6.22 Geometry for benchmarking Monte Carlo coincidence simulation 85

Figure 6.23 CEARXRF simulated singls spectrum compared with the measured singles spectrum with Ge detector 86

Figure 6.24 CEARXRF simulated coincidence spectrum compared with the measured coincidence spectrum with Ge detector 86

Figure 6.25 CEARXRF simulated coincidence spectrum compared with the experimental diagonal summing coincidence spectrum 87

Figure 6.26 Geometry plot for X-ray coincidence measurement of lead in bone with the proposed X-ray coincidence spectrometer 87

Figure 6.27 Geometry plot for X-ray coincidence measurement of lead in bone with the small

X-ray NaI(Tl) detector and the low energy Ge detector.....88

Figure 6.28 X-ray coincidence spectra comparison for lead in bone measurement.....88

1. Introduction

1.1. Overview

X rays, which cover the energy range of 10^2 eV ~ 10 GeV of the whole spectrum of electromagnetic radiation, were discovered by Prof. Wilhelm Conrad Röntgen on November 8, 1895 at the University of Würzburg in Germany (Bertin 1978). Ten Nobel Prizes have been rewarded to researchers for their X-ray related work since the first one to Röntgen in 1901. Characteristic X rays of chemical elements produced by inner shell transitions (10^{-1} keV ~ 10^2 keV), have been studied extensively over the past century, which evolves the discipline of X-ray spectrometry for multi-elemental analysis of materials. Descriptions about the chronological history and essentials of X-ray spectrometry can be found in several classical textbooks (Herglotz and Birks 1978; Jenkins et al. 1981; Jenkins et al. 1995; Jenkins and Vries 1970; Williams 1987).

The advancement of X-ray spectrometry was based upon continuously improved physical understanding of the X-ray emission and interaction mechanism with surrounding materials (specimen). When an incoming photon falls onto a specimen, one of three basic interactions may occur: Rayleigh scattering (coherent scattering), Compton scattering (incoherent scattering) or photoelectric absorption. For scattering interactions, the photon

changes direction according to certain distribution and loses energy for the Compton scattering case. After absorption (figure 1.1a), the target atom is excited by absorbing the photon energy with an inner-shell electron. This electron will be excited out of the shell with the incident photon energy greater than its bounding energy, and leave a core hole in the shell. This core hole will then be occupied by another electron from an outer shell accompanied by the emission of a non-radiative Auger electron (figure 1.1b) or an X ray photon (figure 1.1c) and sometimes both (satellite lines). The X-ray energy from this reaction is discrete and equal to the difference of electron binding energies of those two involved atomic shells, and therefore, they are called characteristic X ray or X-ray Fluorescence (category of luminescence, as apposed to phosphorescence, which is a delayed phenomenon) (Weber 1998). The naming convention of X-ray lines is based on this inter-shell transition

. Figure 1.2 is presented for illustrating this convention (Kortright and Thompson 2002). It is noted that the core hole “transited” to a new shell with lower binding energy than the original shell after the first step of relaxation. With the probability equal to the fluorescence yield of the shell, one more X-ray line with less energy is emitted from the atom in the second step of relaxation, which is the fundamental physics basis of the proposed X-ray coincidence spectroscopy in this thesis.

Since the advent of lithium drifted silicon detectors and germanium detectors in the early 1970s, which offered very good energy resolution for the multi-channel analysis, the

energy-dispersive X-ray fluorescence (EDXRF) measurement has been applied in a wide range, (material analysis, exploration, mining, metallurgy and environmental studies), with advantages of being flexible and fast (Jenkins et al. 1995).

It is well known that lead is a toxic chemical element with irreversible neurological effects, which accumulates in human bones after ingestion or inhalation (Barry 1975; Barry 1981; Barry and Mossmann 1970). The *in vivo* measurement of lead in bone is fundamental for monitoring the lead contamination level of human being. With features being non-destructive and accurate, the EDXRF technique has been applied to *in vivo* bone lead measurement by researchers over the past few decades (Ao et al. 1995; Ao et al. 1997b; Ao et al. 1999a; Ao et al. 1999b; Chettle et al. 1991; Lee et al. 2001; Todd 2000).

Generally speaking, for EDXRF measurement, photons are detected by an energy-dispersive spectrometer capable of resolving X-ray lines according to their energy. Their intensities are recorded in the form of a pulse height spectrum. Elemental compositions can then be obtained by applying quantitative EDXRF analysis methods. In this thesis, the Monte Carlo – Library Least-Squares (MCLLS) method was successfully applied to this application and further improved by incorporating the Differential Operator method (MCDOLLS). X-ray coincidence spectroscopy was also studied to improve the measurement sensitivity by minimizing the detection of back-scattered source photons.

1.2. Review of EDXRF Analysis Methods

For those traditional EDXRF analysis methods, two steps are needed to make quantitative analysis (He 1992). The intensity or intensity ratios of photoelectric peaks of those X-ray lines from elements of interest in the sample are estimated in the first step. Secondly, peak intensities are related to elemental weight fractions by matrix effect correction methods.

For obtaining intensity ratios, four methods, (namely, spectrum stripping, peak integration, deconvolution and least-squares fit), are used primarily. Spectrum stripping is not very accurate and also difficult to use since errors accumulate as the stripping proceeds. Integration and deconvolution basically share the same principle but are applied differently. They both use a detector response model to mathematically calculate the peak intensity. The accuracy of these two methods depends on the accuracy of the detector response model. Limited by their functionality, overlapping peaks can not be resolved by these two methods and only parts of the spectrum information are used. The least-squares fit method solves the problem but introduces new difficulty of experimentally acquiring elemental library spectra, which are the key part of the least-squares fit method.

The matrix effect correction for the quantification of elemental weight fractions can be handled with one of two methods: the empirical coefficients method and the fundamental parameters method. Detailed review for empirical coefficients method can be found in (Bertin 1978; Jenkins 1988). The disadvantage lies in the requirement of measurements on a number of carefully prepared standard samples to determine the empirical coefficients, which is very time consuming and expensive. And quite often, these empirical coefficients are system specific and not transferable to other systems. The fundamental parameters method was initially proposed in the early of 1950s' and invested further (Criss and Birks 1968; Gillam and Heal 1952), which attempts to model the sample matrix effect with a complete mathematical model. In principle, the fundamental parameters method is an absolute method and does not require measurements on standard samples. However, since calculations required are extremely complex, the practical application of this approach usually makes use of pure element standards and the X-ray intensity ratio, that of the unknown sample to that of the pure element standard, to cancel some number of unknown fundamental parameters that are required and simplify the calculation. So, these methods are not absolute.

In addition to these traditional quantification methods, the Monte Carlo - Library Least-Squares (MCLLS) method was proposed by the Center of Engineering Applications of Radioisotopes (CEAR) group and has been applied to research works in EDXRF and Prompt Gamma Neutron Activation Analysis (PGNAA) successfully (Ao et al. 1999a; He et al. 1993;

Shyu et al. 1993; Verghese et al. 1988). This method first requires initial guess values of elemental compositions of the unknown sample. Then the sample spectrum and elemental library spectra are simulated with Monte Carlo simulation codes modeling the required experimental source-sample-detector geometry. Thirdly, elemental weight fractions are obtained by least-squares fit. If fit results largely deviate from initial guesses, iterations will be continued by running the Monte Carlo simulation again with new guess values until correct weight fractions are determined. Advantages of this method lie in the simplicity; resolution of overlapping peaks, utilizing the whole spectra and automatic correction of the matrix effect. It is also noted that the problem with K-alpha to K-beta X-ray ratios is dealt with automatically. In this thesis, the MCLLS method was successfully applied to the *in vivo* XRF measurement of lead in bone, with results presented in chapter 3.

Based upon the iterative nature of the MCLLS method, accurate quantitative results are guaranteed after possibly several iterations. To increase the efficiency of this method, combined with the Differential Operator method, the MCDOLLS method was proposed and studied in this thesis. With the MCDOLLS method, additional data, differential responses of both sample and library spectra, are simulated with the Monte Carlo code. When needed according to new estimated values of elemental weight fractions, simulated sample and library spectra can be re-adjusted with Taylor series expansion without running the Monte Carlo simulation again. This Taylor series re-adjustment process can be repeated until

accurate determination is reached. Obviously, the run time of Taylor series re-adjustment (several seconds) is trivial compared to the run time of the Monte Carlo simulation code (in the order of 10 hours). Chapter 5 describes details about the combination procedure and analysis results.

1.3. X-Ray Coincidence Spectroscopy

The up-to-date EDXRF spectrometers have focused primarily on detecting individual X-ray incidence events with the loss of time correlation information, to which all methods in section 1.2 are applicable. With the objective of improving measurement sensitivity by minimizing back-scattered source photon background, X-ray coincidence spectroscopy was proposed and studied in this thesis.

According to previous work (Ao et al. 1995; Ao et al. 1997a; Ao et al. 1999a; Ao et al. 1999b; Lee et al. 2001), the main interfering background for lead in bone measurement is from back-scattered source photons (figure 1.3), which are also the main problem for the improvement of measurement sensitivity. Based on the physics of the inner-shell atomic transition, certain fractions of the K-series X-ray emission events, determined by the relative yields of all K lines and fluorescence yields of L shell (about 30% for lead), are followed by the emission of L-series X rays in true coincidence within 10^{-15}s (Everett and Cashwell 1973;

Scofield 1974b). With an advanced data acquisition and control system, coincidence experiments were studied and were used to benchmark the Monte Carlo coincidence simulation in chapter 6. An optimal X-ray coincidence spectrometer is proposed and investigated with the benchmarked Monte Carlo simulation code CEARXRF.

1.4. Monte Carlo Simulation Code - CEARXRF

With the help of faster computers and improved physics models, the Monte Carlo simulation method is becoming more and more important in many fields of design and analysis.

CEARXRF, a FORTRAN code for Monte Carlo simulation, has been developed and continuously improved by researchers of the CEAR center (Ao et al. 1997a; Guo et al. 2003; He et al. 1991; Lee et al. 2001). CEARXRF was implemented on Sun Unix workstations in FORTRAN 77 and ported to the Cygwin platform of PC Windows system.

Major motivations of developing CEARXRF are:

- Simulating Monte Carlo elemental library spectra for the quantitative EDXRF multi-elemental analysis
- Investigating the matrix effect with simulated differential responses of sample

and library spectra

- Optimizing the EDXRF spectrometer configuration by improving the measurement sensitivity, which can be done by analyzing series of simulated sample spectra, reliable and accurate approximations of experimental spectra with CEARXRF benchmarked by experimental data

Improved by the work of this thesis, not only the sample spectrum is simulated but also Monte Carlo library spectra for constituent chemical elements of the sample. Moreover, differential responses of sample and elemental library spectra to variations of elemental weight fractions can also be simulated for possible follow-up spectra re-adjustment based upon library least-squares fit results. Chapters 3, 4 and 5 are devoted to introduce this serial of analysis methods in more detail.

For optimizing the X-ray coincidence spectrometer, the coincidence simulation capability has been implemented and benchmarked with the CEARXRF code, which is discussed in chapter 6.

More detailed descriptions about the CEARXRF Monte Carlo simulation code are available in Chapter 2.

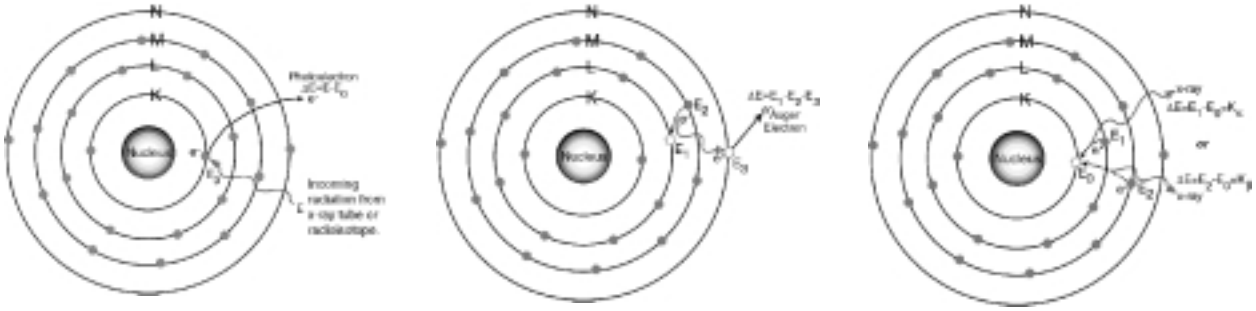

(a) (b) (c)

Figure 1.1 Schematics of characteristic X-ray emission and competing Auger electron process

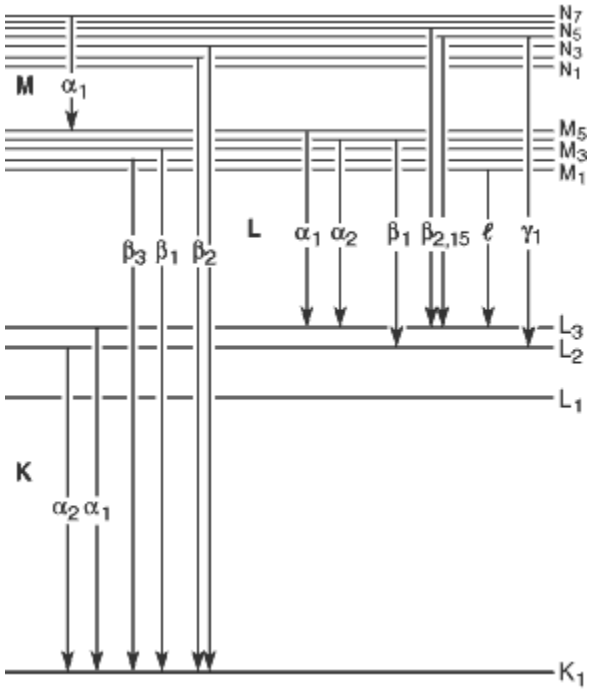

Figure 1.2 Schematics of atomic shell structures and naming conventions for X-ray lines

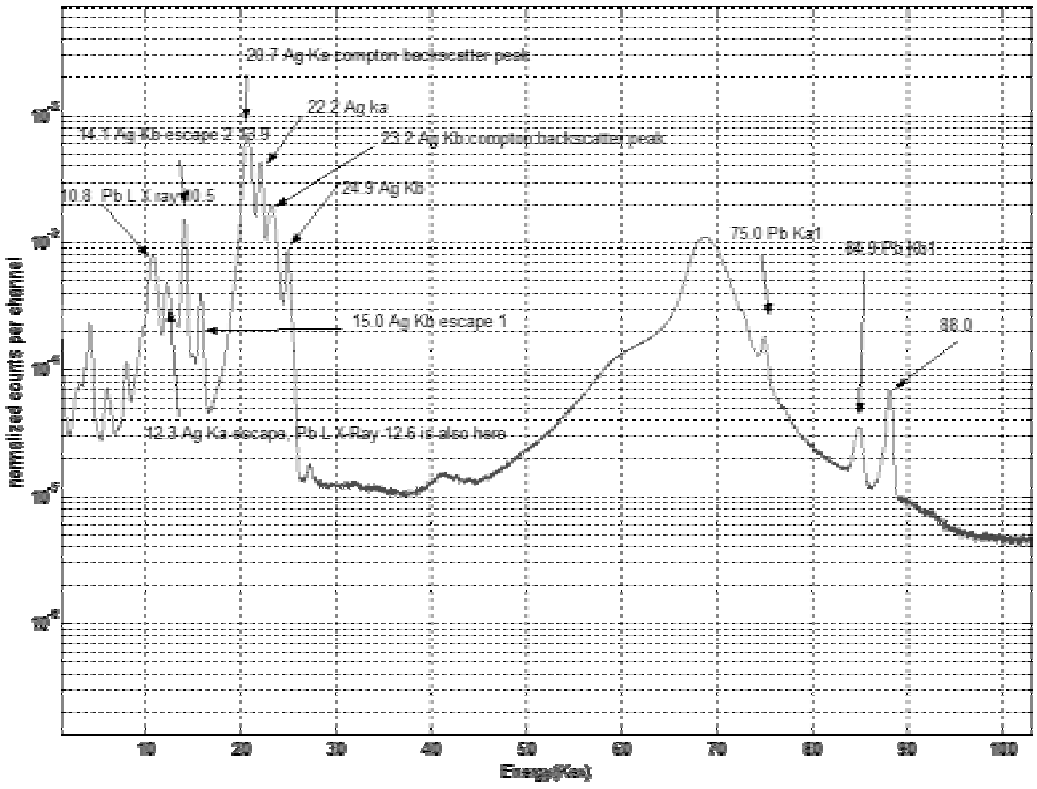

Figure 1.3 *In Vivo* EDXRF experimental spectrum for lead in bone measurement with low energy Ge detector and Cd-109 radioisotope activation source

2. Monte Carlo Simulation Codes – CEARXRF and CEARXRC

2.1. Overview

The energy-dispersive X-ray fluorescence (EDXRF) measurement has been applied in engineering and medical fields for a long time. For the development of an EDXRF spectrometer for these applications, researchers are often required to repeat many 'trial and error' to optimize the system. There are many design requirements that developers of EDXRF spectrometers should optimize through experiments or simulations. Among all these requirements, it is the key factor to improve the minimum detectable concentration (MDC).

Experimental studies for this optimal condition can be very expensive and time consuming. Cases are not rare that it is even not feasible to accomplish all experiments for optimizing the measurement system. With the modern computing facility and detailed physics model, Monte Carlo simulations are playing a more and more important role for system optimization. Monte Carlo simulation results are good approximations for that of measurement, and the use of Monte Carlo codes in the EDXRF spectrometer design and optimization is feasible and has been reported by many researchers (Ao and Gardner 1995; Lee et al. 2001; Lewis 1994; Lewis et al. 1995; Tartari et al. 1991; Todd et al. 1992; Wallace 1994).

Both general purpose Monte Carlo simulation codes, such as EGS4 (Electron Gamma Shower) (Nelson et al. 1985), and MCNP (Monte Carlo N-Particle) (Briesmeister 2000), and specific purpose Monte Carlo codes for EDXRF applications like CEARXRF may be used for simulating EDXRF spectrometers. As a comparison, Table 2.1 briefly summarizes key features of the CEARXRF code and other general purpose Monte Carlo codes with respect to the EDXRF simulation.

The CEARXRF code is not only an important tool for optimizing spectrometers, but also it produces important data for quantitative multi-elemental analysis and X-ray coincidence spectroscopy. These unique and important features include the following:

1) Elemental library spectra simulation for the MCLLS method to quantify elemental compositions of the sample
2) Generation of sample and library differential responses for MCDOLLS analysis
3) X-ray coincidence simulation (CEARXRC is named for the CEARXRF code with coincidence simulation capability)

The detailed features of CEARXRF & CEARXRC codes are introduced in following sections. CEARXRC code has all features of CEARXRF code, except that CEARXRC is capable of Monte Carlo coincidence simulation.

2.2. Simulation Input and Output

The input data of CEARXRF can be specified easily by using a text file, CEARXRF.INP. The detailed manual for using CEARXRF (Guo 2002) is available from CEAR by request. The geometry is specified in the format as required by the HERMETOR package (Prettyman 1992). Different input cards are available for various purposes, such as source cards for describing source radiation, zone card for describing cell information and material card for specifying multi-elemental compositions of each material. Also the usage of each variance reduction technique can be turned on or off for each cell.

As default, the sample spectrum is always available after simulation. As one quality assurance mechanism, a log file is always generated to report the simulation checklist. Optionally, elemental library spectra, differential responses of both sample and library spectra can be generated. For X-ray coincidence simulation, which can be selected optionally, the 2-D histogram data is available. Another interesting output category of the CEARXRF code is the histogram output with XRF lines only.

2.3. General Geometry

One of the most important components of Monte Carlo simulation is to model the

geometry of the experiment as accurate as possible. A geometry-modeling package, called HERMETOR (Gardner et al. 1988; Prettyman et al. 1990), is used in the CEARXRF code.

HERMETOR allows users to define a complex three-dimensional heterogeneous system through a simple and verifiable input file. An approach that combines the boundary representation technique and the constructive solid geometry technique is used to model the system. Information necessary for particle tracking is easily accessible from Monte Carlo codes through calls to subroutines in the modeling package.

Two important functions necessary for particle tracking are provided by HERMETOR, both of which are independent of sampling schemes and physics of particle transport. Given a spatial position within the modeled system, HERMETOR returns a zone index for identification purpose from which properties of the zone, such as compositions and density, can be queried. Secondly, given the zone index, position, and a direction, HERMETOR returns the distance to the zone boundary in the specified direction. These two functions, when combined with appropriate sampling schemes and physics, can be used to solve most particle transportation problems.

Also, HERMETOR offers the functionality to display the geometry of a modeled system as shown in figure 2.1. The feature is very useful in the design stage of complex radiation

gauges and analyzers.

2.4. Photon Transportation Model

Along these years work of CEAR researchers, the photon transportation model keeps improving and being updated for the CEARXRF code.

Photon cross section data for Rayleigh (coherent) scattering, Compton (incoherent) scattering, and photoelectric absorption is incorporated from Storm's data (Storm and Israel 1967) which are essentially the same data found in MCNP 4B (Briesmeister 1997). All chemical elements of interest (Z=1-94) are covered in the energy range of 1 keV to 150 keV.

The angular distribution of scattered photons is sampled for direction and energy of photons after scattering. For coherent scattering, the differential Thomson cross section modified by atomic form factors was implemented (Hubbell 1975). For incoherent scattering, the differential Klein-Nishina cross section modified by incoherent scattering functions (Hubbell 1975) was employed. Also, the Doppler broadening effect, on incoherently scattered photons due to bound electron momentums, was considered through the use of Compton profile data by (Biggs et al. 1975).

To simulate detailed physics of all K and L fluorescence emission lines, shell-wise photoelectric absorption cross section data for K, L1, L2 and L3 shell electrons were adopted from the ENDF/B-VI library (Rose 1991) maintained by the National Nuclear Data Center. Auger, Coster-Kronig, and total fluorescence yields for K, L1, L2 and L3 shells are from (Krause 1979). K and L emission rates that determine the branching ratio of the individual fluorescence line are from (Scofield 1974a; Scofield 1974b). Ionization energy levels are from Bearden's work (Bearden and Burr 1967).

These physics data libraries, available in the current version of CEARXRF, are also listed in table 2.2 with references and comments.

For the Monte Carlo simulation process, these physics data are accessed very frequently for every photon history track. With the total history number in the order of 10^7, the disk access time can be considerably long. To accelerate the simulation process by fast accessing these physics data, two important data structures were implemented in the CEARXRF code.

The first one is the multi-layer indexing technique. For the storage of each category of physics data, such as elemental cross section and the material composition list, one more layer of information is supplied with an array of very small size. This array works as pointers to the related data for each involved chemical element. By doing so, the search time of data

location is greatly reduced.

The second one is the caching technique. Some amounts of those most recently accessed data are stored in a fairly small array as a function of the material and the photon energy. Given the fact of high probability of Rayleigh scattering for the low energy photon, after which the photon only changes flying direction, this technique improves the simulation efficiency in a significant amount.

2.5. CEARXRC - Monte Carlo Coincidence Simulation

To make Monte Carlo simulation for X-ray coincidence measurement, the CEARXRC code was engineered by updating the CEARXRF code.

Based on the physics of X-ray coincidence, L X ray might be emitted after the emission of K X ray with the probability of L shell fluorescence yield. This coincidence phenomenon is simulated by the CEARXRC code in the exactly same way as this physical process. To make this work, several sets of memory space were allocated.

The first set of memory is for logic flags for each history. It marks the occurrence of a coincidence photon. At the end of simulation for each photon, this flag will be queried. If it

indicates that there are more coincidence photons to be processed, the coincidence handler will be responsible for setting parameters for the coincidence photon and submitting it to the main history tracker. It also clears the flag after all coincidence photons are processed.

The second set of memory is allocated for storage of coincidence photon parameters, such as spatial location, flight direction and energy information. This set of data is used by the coincidence handler for setting parameters for the coincidence photon before submitting it to the main history tracker.

The third set of memory is used for detector scoring. The score of each detector for the current history is stored in the cache array before simulation for all coincidence photons of one history are finished. At the end of the complete simulation of each history, this set of data is used for an indication of coincidence detection, which simply means that both detectors have score greater than zero. Also, this set of data is used for updating both singles and coincidence histogram. For this purpose, four cases were treated differently.

1. Coincidence photons are detected by two detectors separately. Both singles histogram and coincidence histogram will be updated for this case. The formula for updating is: $W_C = W_K * W_L$ / Wparent; $W_{s1} = W_K$; $W_{s2} = W_L$
2. Coincidence photons are detected both by one single detector. This is the summing case and only the singles histogram for this detector will be updated by:

$W_{s*} = W_K * W_L / Wparent$

3. Only one photon is detected by one of the two detectors and the other one is lost. Only the singles histogram of that detector will be updated with the weight of the photon being detected.
4. The last case is trivial. Both photons are lost and nothing will happen to the histogram.

2.6. Sampling Schemes

- **Source Photon Sampling**

In the CEARXRF code, the initial location, direction and energy (and the polarization vector if needed) of source photons are selected from their own probability distribution function independently. By combining these three variables, various source forms including distributed radioisotope and X-ray tube sources can be simulated with ease.

For sampling the source photon initial location, various shapes of the activation source are selectable from the input source card, which can be a point, circle, ring, rectangle, sphere, cylinder, hollow or a parallelepiped with two general rotation angles (polar and azimuthal rotations). The source photon direction can be specified as isotropic, mono-directional, or

cone beam source with a few biasing schemes. Source energy distributions can be discrete, continuous (spectral information input needed), a combination of these, or sampled from an X-ray tube source spectrum (Pella et al. 1985).

- **Path Length Sampling**

In the CEARXRF code, to sample the particle's path length between two consecutive interactions, the length to the boundary of the current zone is calculated with HERMETOR subroutines along the photon flying direction. With cross section data of the zone material and this length data, it is easy to identify whether an interaction will occur or not. If an interaction will occur, the path length is sampled according to biasing options as specified, otherwise, travel of the photon in the next zone will be tracked similarly until an interaction occurs or the escape zone is reached.

- **Colliding Element Sampling**

If a collision occurs in a zone that consists of more than one chemical element, the colliding element is sampled uniformly with the true probability for each chemical element as following:

$$p_i = \Sigma_i \Big/ \sum_{j=1}^{m} \Sigma_j$$

where Σ_i is the total macroscopic cross section of the i-th element and m is the total number of elements in the zone.

- **Interaction Type Sampling**

The true probability distribution function for sampling the interaction type for a given chemical element is:

$$p_i = \sigma_i \Big/ \sum_{j=1}^{k} \sigma_j$$

where σ_i is the microscopic cross section for the i-th interaction type and k is the number of interaction types with photon for that chemical element.

- **Scattered Direction and Energy Sampling**

Two types of scatter interactions are possible for the low energy photon, Rayleigh scatter (coherent scatter) or Compton scatter (incoherent scatter).

The coherent scatter is important at low energies and for high Z elements when the electron must be considered bound. Only the photon direction is changed after the collision.

For this interaction, the differential scattering cross section is given by

$$\sigma_c(Z,\alpha,\mu)d\mu = C^2(Z,w)T(\mu)d\mu$$

where $C(Z,w)$ is the atomic form factor and w is the inverse length as a function of α and μ.

$$w = k\alpha(1-\mu)^{1/2}$$

where k is equal to 29.1433 (1/cm).

The energy-independent Thomson differential scattering cross section can be expressed as

$$T(\mu)d\mu = \pi r_0^2(1+\mu^2)d\mu .$$

The general effect of $C^2(Z,w)$ is to decrease the Thomson cross section more extremely for backward scattering, high energy, and low Z elements.

Sampling the cosine of the scattering angle, μ, can be transformed to sample w^2

(Carter and Cashwell 1975)

$$p_c(w) = C_2\left[\frac{1+\mu^2}{2}\right]\frac{C^2(Z,w)Z^{-2}}{I(Z,w^2)}$$

where C_2 is a normalization constant for given Z and α. By using a generalized rejection technique, the $C^2(Z,w)Z^{-2}/I(Z,w^2)$ can be sampled and thereby the direction of the scattered photon.

Photon scattering from free electrons is referred to as incoherent scattering since the independent behavior of the electrons prevents any interference effect. For this interaction, the differential scattering cross section is in the form

$$\sigma(Z,\alpha,\mu)d\mu = S(Z,w)K(\alpha,\mu)d\mu$$

where $S(Z,w)$ is the incoherent scattering function modifying the Klein-Nishina differential cross section

$$K(\alpha,\mu)d\mu = \pi r_0^2\left(\frac{\alpha'}{\alpha}\right)^2\left(\frac{\alpha'}{\alpha}+\frac{\alpha}{\alpha'}+\mu^2-1\right)d\mu$$

where Z is the atomic number, μ is the cosine of the scattering angle, α and α' are ratios of the photon energy before and after scattering to the rest mass energy of the electron respectively, r_0 is the classical Thomson radius of the electron, and w is the inverse length defined as previous for coherent scattering.

Qualitatively, the effect of S(Z,w)/Z is to decrease the Klein-Nishina cross section more extremely in the forward direction, for low energy and for high elements independently.

The probability for sampling the cosine of the scattering angle, μ, is

$$p_i(\mu) = \frac{S(Z,w)K(\alpha,\mu)}{\sigma_i(Z,\alpha)} = C_1 \frac{S(Z,w)K(\alpha,\mu)}{S(Z,\overline{w})\sigma_k(\alpha)}$$

where $\sigma_i(Z,\alpha)$ and $\sigma_K(\alpha)$ are the microscopic incoherent scattering cross section and the integrated Klein-Nishina cross section, respectively, C_1 is a normalization constant larger than one for given Z and α, and $\overline{w}$ is the maximum value of w for a given α. The term $S(Z,w)/S(Z,\overline{w})$ is in the interval [0,1] since S(Z,w) is a monotonic increasing function of w for a given Z. The directional cosine of the scattering angle, μ, can be sampled using a generalized rejection technique (Carter and Cashwell 1975). This is done by calculating the inverse length, w, from the inverse equation described above for the given photon energy after choosing the scattering angle from the Klein-Nishina cross section pdf,

$K(\alpha,\mu)/\sigma_K(\alpha)$. Next it is used to obtain the value of the scattering function, S(Z,w), by interpolation for a given Z. Finally, if a uniform random number is less than $S(Z,w)/S(Z,\overline{w})$, the scattering angle is accepted; otherwise it is rejected, and the procedure is repeated.

- **X-Ray Fluorescence Sampling**

When a photoelectric absorption occurs, the interaction probability of each shell is determined by:

$$P_i = \frac{\sigma_i(E)}{\sigma^{pe}(E)}$$

where i indicates K, L1, L2 or L3 shell, $\sigma_i(E)$ is the photoelectric absorption cross section of the i-th shell and $\sigma^{pe}(E)$ is the total photoelectric absorption cross section.

When the selected core hole occurs at shells other than K and L shells, the photon is killed because M-series and outer shell X rays have very low energy and they are rarely useful for EDXRF applications, consequently they are not treated in the CEARXRF code.

When the core hole occurs at K or L shell, then one X-ray line, with the possibility equal

to the fluorescence yield of the shell, is picked according to the relative intensity data. This generates a new core hole in an outer shell, if this shell is one of the three L shells, another X-ray line is picked similarly and all parameters necessary for tracking it are stored. If the coincidence simulation option is turned on, this coincidence photon will be tracked in the same way as tracking the first X-ray photon. If these two photons are detected by two detectors separately, one coincidence event will be logged in the 2-d histogram storage.

2.7. Variance Reduction Techniques

For Monte Carlo simulation, one way is to simulate the photon history strictly based on the true probability distribution function of each event, which is known as analog simulation. The advantage of analog simulation is that it is intuitive and simple, also more reliable. But the problem is that the simulation process would have to be very long so that the statistics of simulation results are good enough, sometimes it is not even feasible due to some restrictions. The other way is by using some so-called variance reduction functions, those events, which have more dominant effect on simulation results, are sampled more “preferably” and with the “weight” of events adjusted accordingly to guarantee accuracy. Variance reduction techniques have been proven to be powerful and effective for Monte Carlo simulation and they take important roles in the CEARXRF code.

- **Stratified Sampling**

To improve the statistics of characteristic X-rays for those trace elements, at each interaction site, all possible characteristic X-rays of all chemical elements in the cell are forced to be emitted and a proper weight adjustment is made for each emitted X-ray photon (Cashwell and Everett 1959).

Assume W_0 is the source photon weight before a photoelectric interaction is forced to occur, the weight of each resulting photon is:

$$W_{ij} = W_0 \times \frac{\Sigma_{ai}}{\Sigma_T} \times \frac{\Sigma_j}{\Sigma_{ai}} \times \omega_{ij} \times \eta_{ij}$$

where Σ_{ai} is the macroscopic photoelectric absorption cross section of the i-th element in the cell; Σ_T is the total macroscopic cross section of all elements in the cell; Σ_T is the shell-wise macroscopic photoelectric absorption cross section for the j-th X-ray to be emitted; ω_{ij} is the fluorescence yield of the i-th element at the shell for the j-th X-ray to be emitted; and η_{ij} is the characteristic X-ray yield of the j-th X-ray relative to all other lines in the same series.

- **Correlated sampling**

The correlated sampling technique (Gardner et al. 1989) is a partially deterministic method that is accomplished by making the normal Monte Carlo simulation on a reference sample and then forcing the same particle path in a number of comparison samples that contain zones of different composition and density. This is done by making appropriate weight corrections for the comparison samples. These weight corrections are for the distance to collision site and the collision element. This implies that these comparison samples must contain all the elements contained in the reference sample. When this is not the case one must include very small pseudo amounts of the element or elements in question. The additional computation time required to simulate comparison samples is comparatively small, typically in the order of 20% for twenty comparison samples (Lee et al. 2001).

- **Energy Cutoff**

The photon history or the photon tracking process is also terminated when its energy falls below a specified energy threshold. The basis of the cutoff is that the lowest energy of interest is about 1 - 2 keV in EDXRF applications. The advantage is that it saves simulation time per history since it is unnecessary to track the photon history below this energy threshold.

- **Direction Biasing**

To increase the possibility of source photons flying into the sample, the source direction can be optionally biased in the direction of the source collimation instead of being selected isotropically. An exponential distribution or a combination of cone beams can be used as the biased source probability distribution function, which may allow more than 90% of the source photons to be emitted toward the sample from the source collimator with the photon weight adjusted accordingly.

- **Russian Roulette**

First a minimum weight is set and if the particle weight is lower than this minimum weight, a uniform random number ξ between 0 and 1 is sampled. Then the value of ξ is compared with the preset constant between 0 and 1 (such as 0.2). Particle survives with a weight equal to the multiplication of original weight and the inverse of the preset constant (1/0.2=5) if the value of random number ξ is less than the preset constant. Otherwise the particle is killed and the history is terminated.

2.8. Experimental Benchmark

The CEARXRF code has been benchmarked after each major modification over past

years (Ao et al. 1997a; He et al. 1991; Lee et al. 2001). In this thesis, the benchmark experiment was carried out with the geometry shown in figure 2.2, in which the source-sample-detector angle was 120±10 degrees, as illustrated in the figure. A low energy Germanium detector was used (table 2.3). The experimental sample was made of the Plaster of Paris, with certified elemental weight fractions of hydrogen (0.6630%), carbon (0.5076%), oxygen (49.9990%), silicon (0.4874%), sulphur (20.8000%), calcium (27.2737%), iron (0.0839%), strontium (0.1691%), and lead (162 μg Pb / g Plaster). The density of the sample is $1.850\,\mathrm{g}/cm^3$. The simulated spectrum is compared with the experimental spectrum in figure 2.3. Generally speaking, they show very good agreements in the full spectrum range. There are several potential sources of discrepancies, which are listed in the order of importance:

- Inexact estimation of the background; the background is higher in the high-energy range than it is in the low-energy range
- Pulse pile-up
- Imperfect modeling of the collimator used for the experiment
- Errors in the semi-empirical model used to estimate the resolution of the detector as a function of energy
- Geometry arrangement differences between the experiment and the simulation

Table 2.1 Comparison table for features of CEARXRF and other general purpose Monte Carlo simulation codes

CODE	CEARXRF	EGS4	ITS 3.0	MCNP 4C
Establishment	NCSU, USA	SLAC, USA KEK, Japan NRCC, Canada	SAND, USA	LANL, USA
Particles	Photon	Photon/Electron	Photon/electron	Neutron/Photon/electron
Elements(Z)	1-94	1-100	1-100	1-94
Energy Regime	1-150 kev	1kev – 100Gev	1kev-100Gev	1kev-100Gev
XRF Physics	All K and All L	$K_{\alpha 1}, K_{\alpha 2}, K_{\beta 1}, K_{\beta 2}$ and L	All K and L, Average M and N	$K_{\alpha 1}, K_{\alpha 2}, K_{\beta 1}, K_{\beta 2}$ and average L
Photon Physics	PE, Incob, Coh, Doppler, Polarization	Same + Pair	Same-Doppler Polarization	Same
Geometry	General	General	General	General
Variance Reduction	Powerful for XRF	Basically analog	Few and simple	Powerful for transport analog for spectra
Correlated Sampling	Yes	No	No	Yes (from 4B)
Library spectra	Yes	No	No	No
Differential Responses	Yes	No	No	No
X-ray Coincidence simulation	Yes	No	No	No

Table 2.2 Table for physics data library used by CEARXRF and related references

Physics		References	Comments
Photo-electric total absorption cross section		(Storm and Israel 1967)	Same as MCNP 4B data
Coherent Scattering	**cross section**	(Storm and Israel 1967)	Same as MCNP 4B data
	Angular Distribution		Differential Thomson cross section modified by atomic form factors, tabulated as a function of momentum transfer in the CEARXRF cross-section tables
	Atomic Form Factors	(Hubbell 1975)	
Incoherent Scattering	**cross section**	(Storm and Israel 1967)	Same as MCNP 4B data
	Angular Distribution		Differential Klein-Nishina cross section modified by incoherent scattering function, tabulated as a function of momentum transfer in the CEARXRF cross-section tables
	Incoherent Scattering Function	(Hubbell 1975)	
	Doppler broadening effect	(Biggs et al. 1975)	Detailed formula can be found in Dr. He's thesis P56
Shell-wise photoelectric absorption cross sections		(Rose 1991)	for K, L1, L2, L3, ENDF/B-VI database
Auger, Coster-Kronig, and total fluorescence yields		(Krause 1979)	for K, L1, L2, and L3 shells
K and L emission rates		(Scofield 1974a; Scofield 1974b)	
Ionization energy levels		(Bearden and Burr 1967)	

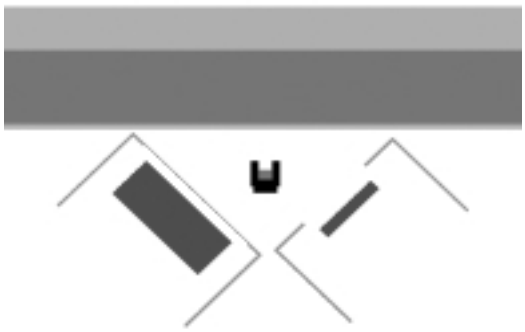

Figure 2.1 HERMETOR geometry plot of the detector-source-sample arrangement for EDXRF measurement

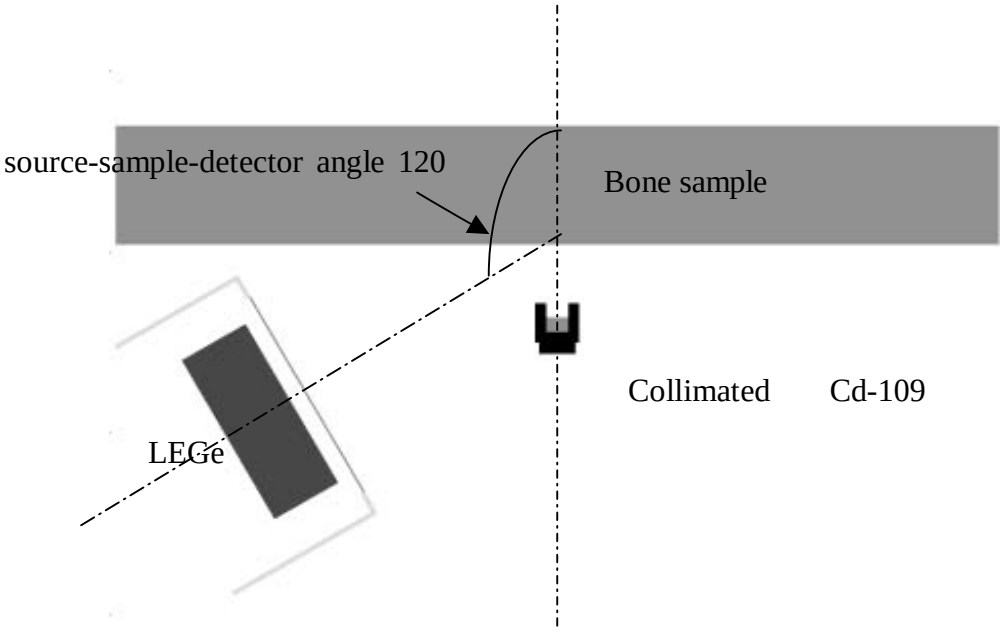

Figure 2.2 Schematics of detector-source-sample geometry for benchmarking the CEARXRF simulation applied to *in vivo* lead in bone measurement

Table 2.3 Low energy Germanium detector characteristics pertinent to this thesis

Active crystal area (mm^2)	2000
Active crystal radius (mm)	25.2
Crystal thickness (mm)	15
Window material	Be
Window thickness (mm)	0.5
Window to crystal distance (mm)	5

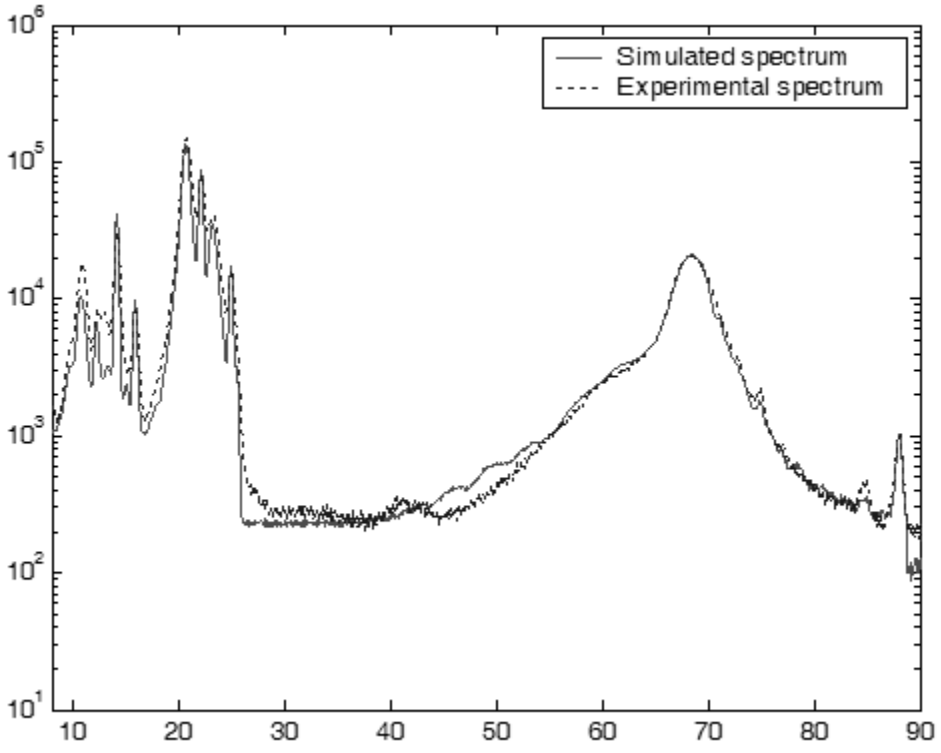

Figure 2.3 CEARXRF simulated sample spectrum compared with the experimental sample spectrum

3. Monte Carlo - Library Least-Squares Method (MCLLS)

3.1. Overview

With the MCLLS method, a measured spectrum of an unknown sample can be described as a linear combination of elemental library spectra constituting the sample:

$$R_{s,i} = \sum_{j=1}^{n} \alpha_j R_{e,j,i} + e_i$$

where $R_{s,i}$ is the sample counting rate in the i-th channel, α_j is the weight fraction of the j-th element of the sample, $R_{e,j,i}$ is the counting rate in the i-th channel contributed by the j-th element (with matrix effect corrected), and e_i is the error term for the fit of the ith channel. Weight fractions can be obtained by linear least-squares fit to minimize the reduced chi-square value with respect to all elements.

$$\chi_v^2 = \frac{1}{v} \sum_{i=n_1}^{n_2} \frac{e_i^2}{\sigma_i^2}$$

where σ_i is the standard deviation of $R_{s,i}$, v is the degree of freedom, and n_1 and n_2 are the limits of fitting channels. The set of equations for estimating $\sigma(\alpha_j)$ can be found

in the paper by (Arinc et al. 1975).

The fundamental idea of the MCLLS method is to obtain elemental library spectra via Monte Carlo simulation for quantitatively measuring multi-elemental compositions of the unknown sample, instead of doing so by tremendous amount of experiments. Obviously, it is cost and time effective. Not only so, the full advantages of this method will be discussed in the next section.

In this thesis, this method is successfully applied to the *in vivo* EDXRF measurement of lead in bone. Analysis results are presented in section 3.3.

3.2. MCLLS Simulation Procedure and Advantages

The MCLLS method consists of the following steps:

1. By Monte Carlo simulation, the complete pulse height spectrum is generated for a sample of assumed compositions
2. With the Monte Carlo computer code, the individual spectral response for each chemical element of the sample is recorded to provide the library spectral response.
3. The least-squares (linear) fit is used to obtain elemental weight fractions of the unknown sample for which the complete spectral response has been measured.

4. If elemental weight fractions calculated for the unknown sample are not close enough to those assumed for the sample used in the Monte Carlo simulation so that a linear relationship exists, then another Monte Carlo simulation must be performed for an assumed composition closer to that of the unknown sample. The reduced Chi-square value can be used as an indicator that correct compositions have been found.

Compared to those traditional quantitative EDXRF methods, major advantages of this method are:

- Elemental library spectra are acquired by Monte Carlo simulation instead of by extensive and time consuming experiments
- Overlapping peaks in the sample spectrum due to X-ray lines from different elements with close energy values are automatically resolved
- The entire spectrum information is available to be utilized
- The matrix effect is automatically corrected
- The measurement uncertainty is directly available from the least-squares fit

3.3. Application to *In Vivo* Measurement of Lead in Bone

The MCLLS method was applied to *in vivo* lead in bone measurement by quantitatively determining the lead concentration based on the spectrum of the CEARXRF benchmark

experiment in chapter 2. The elemental library spectra were simulated with CEARXRF. They are shown in figure 3.1 together with the simulated sample spectrum.

The library least-squares fit was done for both the simulated sample spectrum (as a quality assurance factor) and the experimental spectrum (the quantification process). Fit results are shown in table 3.1 and table 3.2 respectively. The fitted spectrum is compared with the experimental spectrum in figure 3.2. Clearly, fit results with the simulated sample spectrum are very good and fit results with the experimental spectrum show good accuracy also.

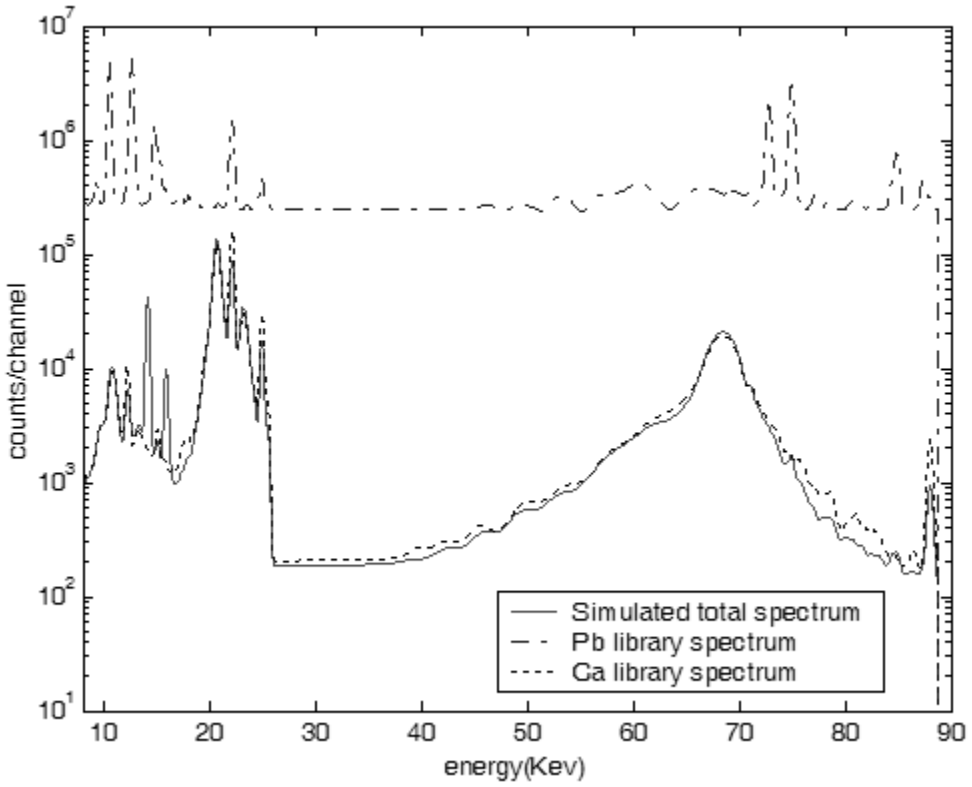

Figure 3.1 CEARXRF simulated sample spectrum and library spectra of lead and calcium for *in vivo* EDXRF measurement of lead in bone

Table 3.1 MCLLS quantitative results for *in vivo* lead in bone measurement by fitting the simulated sample spectrum

	Calculated weight fraction ± RMS	Nominal weight fraction	Relative error between Calculated and nominal values	Correlation coefficient	Reduced Chi-Square
Ca	27.1073%±0.53%	27.2737%	0.61%	0.9660	1.009
Sr	0.1690%±0.16%	0.1691%	0.06%	0.2669	
Pb	0.0164%±0.94%	0.0162%	0.61%	0.2489	

Table 3.2 MCLLS quantitative results for *in vivo* lead in bone measurement by fitting the experimental sample spectrum

	Calculated weight fraction ± RMS	Nominal weight fraction	Relative error between Calculated and nominal values	Correlation coefficient	Reduced Chi-Square
Ca	24.7316%±0.67%	27.2737%	9.3%	0.9068	303.456
Sr	0.1531%±0.17%	0.1691%	9.5%	0.2234	
Pb	0.0185%±0.96%	0.0162%	14.2%	0.2385	

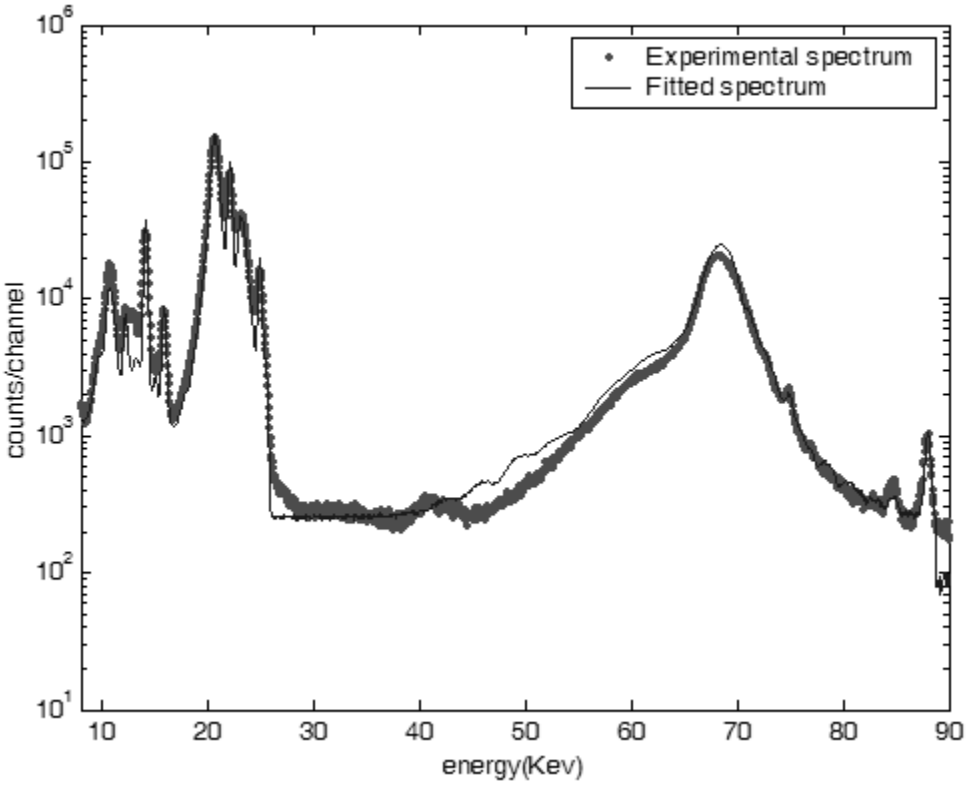

Figure 3.2 MCLLS fitted sample spectrum compared with the experimental spectrum

4. Monte Carlo - Differential Operator Method

4.1. Overview

The Differential Operator method was discussed in literatures (Hall 1982; Rief 1984; Rief 1994), which is very powerful for measurement sensitivity study and system optimization. With the set of equations in the next section, the Monte Carlo - Differential Operator method was implemented in CEARXRF for simulating differential responses of both sample and elemental library spectra. Via the mathematics of Taylor series expansion, these differential responses can be used for spectra re-adjustment according to possible weight fraction differences between initial guess and true values of the unknown sample. Discussed later in chapter 5, the MCDOLLS method, by combining the MCLLS method with the Differential Operator method, turns out to be very promising for quantitative multi-elemental analysis.

4.2. Mathematical Treatment

Mathematically, the spectral response can be expressed as the average value of each photon history weight that is scored by the detector. So, differential spectral responses to variations of elemental weight fractions are also equal to average values of derivatives of

photon weights with respect to variations of elemental weight fractions.

The process of photon history track can be treated as multiple steps. The photon weight is adjusted with a weight correction factor accordingly for each step. The mathematical equation is:

$$w_n = w_{n-1} \cdot f_n$$

So the derivative of the photon weight can be expressed as:

$$\frac{\partial w_n}{\partial \alpha_j} = \frac{\partial w_{n-1}}{\partial \alpha_j} f_n + \frac{\partial f_n}{\partial \alpha_j} w_{n-1}$$

At the end of each step, the incident photon either escapes or reacts with constituent elemental atoms until the history is terminated according to certain rules or scored by a detector. To calculate the derivative of the photon weight, four possible scenarios are considered (Lee 1999) and those related equations are presented in table 4.1.

Case A: Escape, the photon escapes from a region without interaction

Case B: Reaction, path length determination in a region

Case C: Reaction element selection: the interested element is selected

Case D: Reaction element selection: an element other than the interested element is

selected

4.3. Simulated Differential Responses

To verify the implementation of the Monte Carlo - Differential Operator method, one simulation case was carried out with the geometry in figure 4.1. The bone density is $1.850\,\mathrm{g}/cm^3$ with elemental weight fractions of Hydrogen (0.2065%), Carbon (0.5618%), Nitrogen (0.2639%), Oxygen (57.1180%), Sulphur (17.2637), Calcium (24.1050%), Strontium (0.141558%) and Lead (168 ppm). Differential responses of the sample spectrum, Pb library spectrum and Ca library spectrum to weight fraction variations of Pb and Ca are presented from figure 4.2 to figure 4.7.

Qualitatively, the simulated differential responses are explained as below. The quantitative application of differential responses is postponed to the next chapter.

As shown in figure 4.2 and figure 4.3, the sample spectrum has positive differential responses in the Ca characteristic X-ray region due to the increment of Ca elemental weight fraction, which is reasonable due to the increment of Ca macroscopic cross section of photoelectric absorption. Also, it is true that due to the absorption effect of Ca, Pb X-rays have negative responses. This can also show that the matrix effect of the EDXRF

measurement is not negligible. The same argument is applicable to the differential response for the variation of Pb elemental weight fraction. Due to absorption cross-section of Pb and Ca, the back-scattered source Ag X rays give negative responses.

The same explanation can be extended to interpret those simulated differential responses of Ca and Pb library spectra.

Table 4.1 Table of equations for calculating the first-order derivative of weight correction factor to the variation of elemental compositions

Cases	Derivative calculation equations
Case A	$\frac{\partial f}{\partial \alpha_j} = -\sigma_j l$
Case B	$\frac{\partial f}{\partial \alpha_j} = -\sigma_j \left(\frac{1}{\Sigma_0 + \alpha_{0j}\sigma_j} \right) - l$
Case C	$\frac{\partial f}{\partial \alpha_j} = \frac{\Sigma_0}{\alpha_{0j}\left(\Sigma_0 + \alpha_{0j}\sigma_j\right)}$
Case D	$\frac{\partial f}{\partial \alpha_j} = \frac{-\sigma_j}{\Sigma_0 + \alpha_{0j}\sigma_j}$

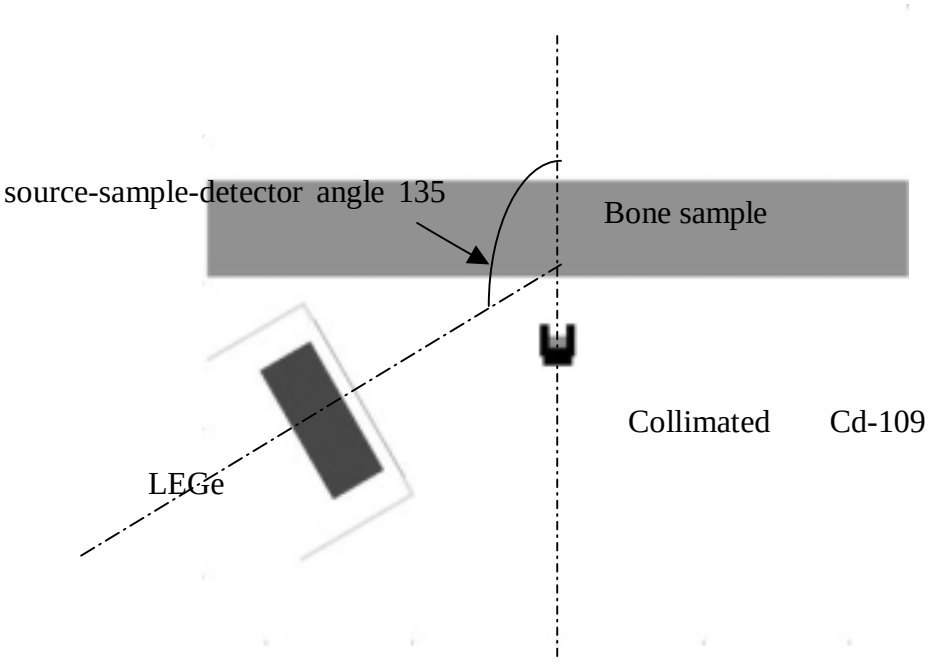

Figure 4.1 Schematics of detector-source-sample geometry for validating CEARXRF simulated differential responses

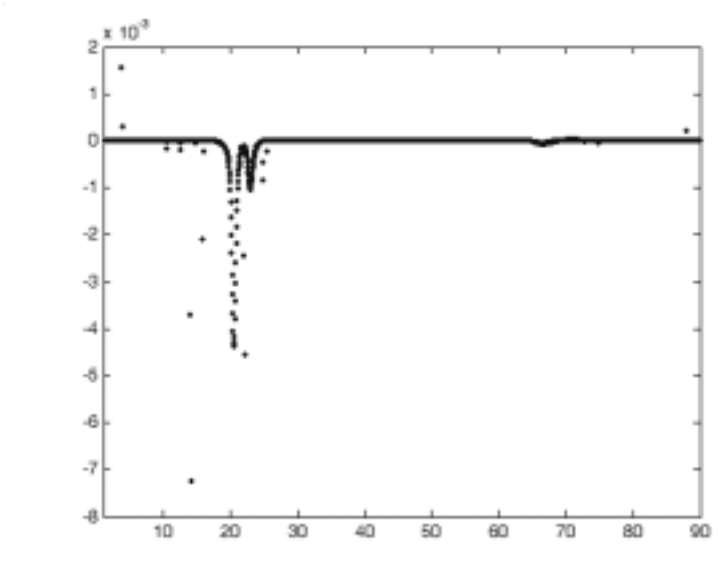

Figure 4.2 Differential response of sample spectrum to the variation of Calcium composition of the sample

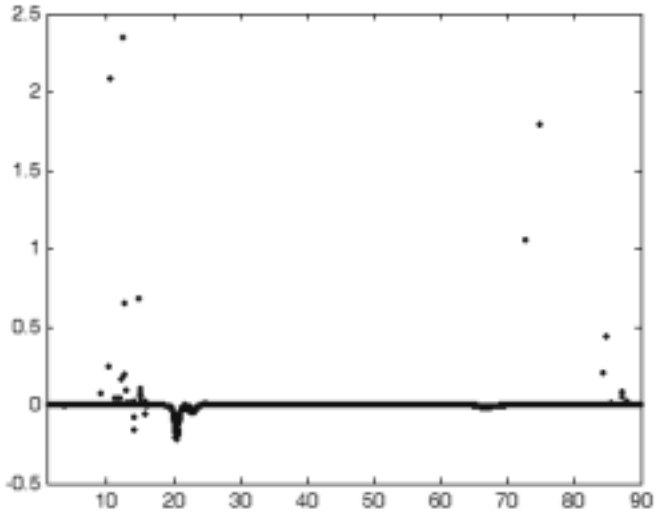

Figure 4.3 Differential response of sample spectrum to the variation of Lead composition of the sample

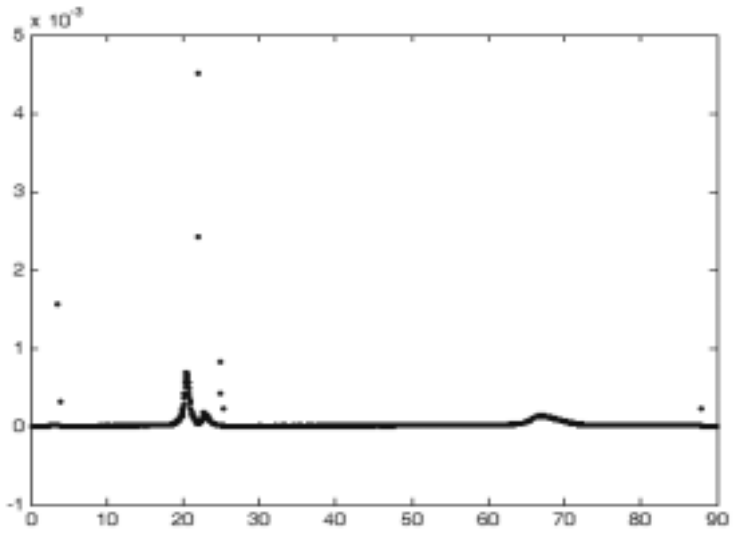

Figure 4.4 Differential response of Calcium library spectrum to the variation of Calcium composition of the sample

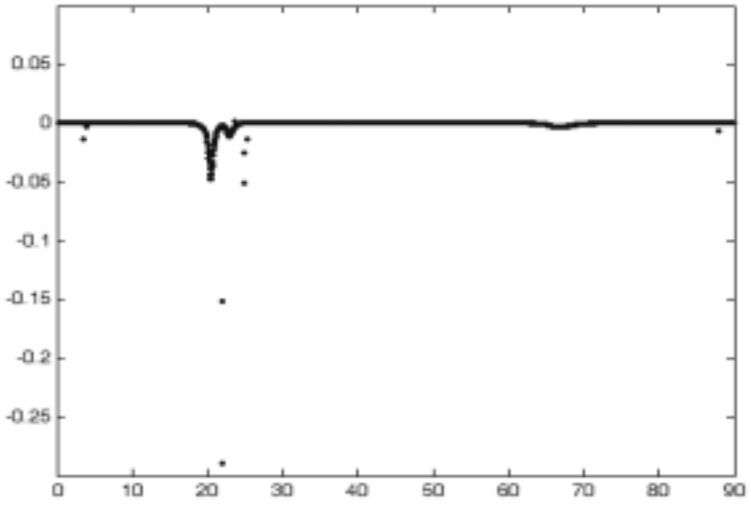

Figure 4.5 Differential response of Calcium library spectrum to the variation of Lead composition of the sample

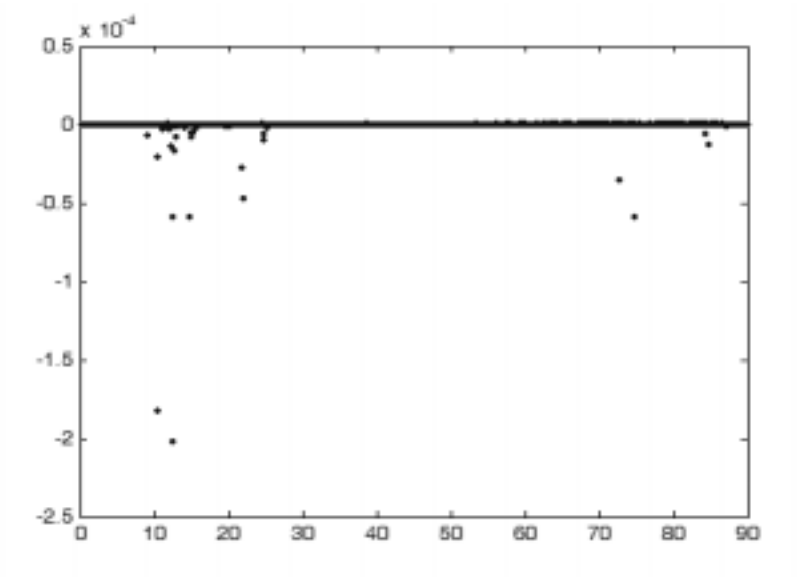

Figure 4.6 Differential response of Lead library spectrum to the variation of Calcium composition of the sample

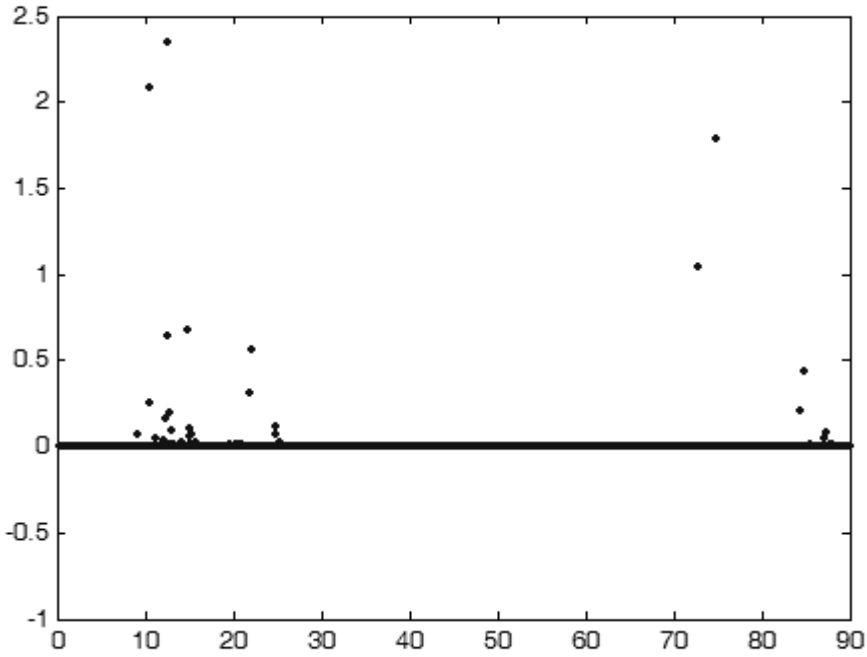

Figure 4.7 Differential response of Lead library spectrum to the variation of Lead composition of the sample

5. MCDOLLS - Combining the MCLLS and Differential Operator Method

5.1. Overview

For the MCLLS method, the initial guess is an important and difficult part to do in practical cases. The estimation method by calculating photoelectric peak ratios the of experimental unknown sample spectrum was used by (He 1992) for cases of analyzing aluminum alloys. This strategy is difficult to be done when those peaks in the sample spectrum overlap with each other as shown in figure 1.3 for the *in vivo* lead in bone measurement. Theoretically, with several iterations, the MCLLS method guarantees reliable results. But the run time of Monte Carlo simulation can be a problem for some possibly on line applications.

To overcome this problem, the MCLLS method was combined with the Monte Carlo - Differential Operator method successfully. This combined method is named as MCDOLLS method. The fundamental mathematics of MCDOLLS is to re-adjust elemental library spectra with the first order Tailor series expansion until fitting results are good enough, as shown in the equation below:

$$R_{s,i}\Big|_{\alpha'} = R_{e,j} + \sum_{j=1}^{n}\left(\alpha'_j - \alpha_j\right)\frac{\partial R_{e,j,i}}{\partial \alpha_j}$$

5.2. MCDOLLS Method Procedure

The MCDOLLS method consists of the following steps:

1. By Monte Carlo simulation, the complete pulse height spectrum is generated for a sample of assumed compositions
2. With the Monte Carlo computer code, the individual spectral response for each element within the sample is recorded to provide library spectral response
3. During the same simulation, differential responses of the sample spectrum and elemental library spectra are acquired
4. The library least-squares (linear) fit is used to obtain elemental weight fractions of the unknown sample for which the complete spectral response has been measured.
5. If these elemental weight fractions calculated for the unknown sample are not close enough to those assumed for the sample in the Monte Carlo simulation so that a linear relationship exists, library spectra are re-adjusted with the Taylor series expansion according to new guess values (close to initial values but deviates from them). The linear fitting is done again until convergence.

5.3. Application to *In Vivo* Measurement of Lead in Bone

To verify the efficacy of the combined method, two cases were simulated with elemental weight fractions listed in table 5.1. The geometry was the same as in figure 4.1. For both cases, differential responses were simulated along with the sample and library spectra. The simulated sample spectra for these two cases are compared in figure 5.1.

After simulations were accomplished, the sample spectrum with 168ppm of lead, applied with Poisson statistics, was considered to be the experimental unknown spectrum. Those elemental library spectra simulated with 1002ppm of lead were used to fit the unknown spectrum. Fitting results are presented in table 5.2. It is clear that fitting results are not good enough due to the great deviation of initial guess values from true values.

Then, those simulated sample and library spectra calculated with 1002ppm of lead were re-adjusted by the Taylor series expansion, with all final weight fractions equal to values of case B respectively for each chemical element of the sample. The re-adjusted sample spectrum is compared with the directly simulated sample spectrum in figure 5.2. It is clear that they are almost identical completely. Re-adjusted Pb and Ca library spectra are also compared with those directly simulated spectra in figure 5.3 and figure 5.4 respectively, which also show very good agreement. The fitting process was done again with these re-adjusted library spectra and results are shown in table 5.3.

Table 5.1 Table of elemental weight fractions of two bone samples studied for MCDOLLS simulation cases

Elements	True Weight Fraction (%)	
	Case A	Case B
H	0.021849	0.021849
C	0.004375	0.004375
N	0.0020675	0.0020675
O	0.554067	0.554067
S	0.174902	0.174902
Ca	**0.240304**	**0.241138**
Sr	0.0014156	0.0014156
Pb	**0.001002**	**0.000168**

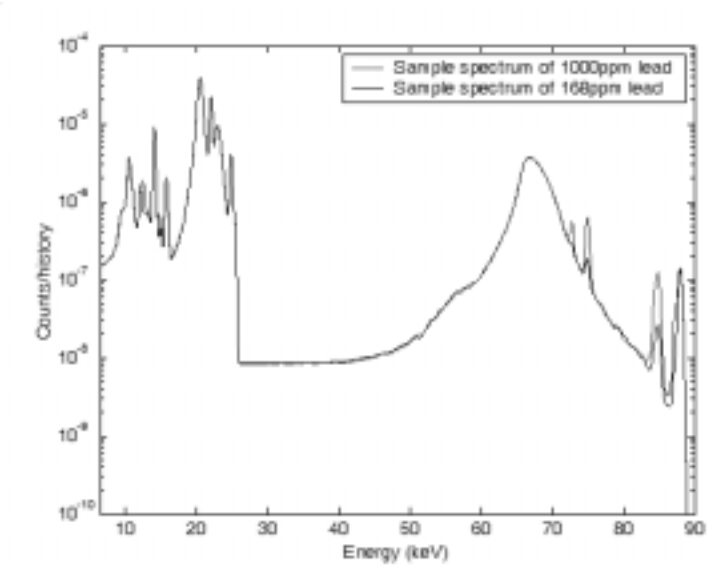

Figure 5.1 CEARXRF simulated sample spectra for validating the MCDOLLS method

Table 5.2 MCLLS quantitative results by fitting sample spectrum of case B with elemental library spectra of case A

Element	Calculated weight fraction (%)	True weight fraction (%)	Relative Error (%)
H	0.000638190	0.021849	97.08
C	-0.109436	0.004375	2601.39
N	0.0333941	0.0020675	1515.19
O	0.776424	0.554067	40.13
S	0.359212	0.174920	105.4
Ca	0.000157428	0.241138	99.93
Sr	0.00142744	0.00141560	0.8
Pb	0.000151290	0.000168	10.0

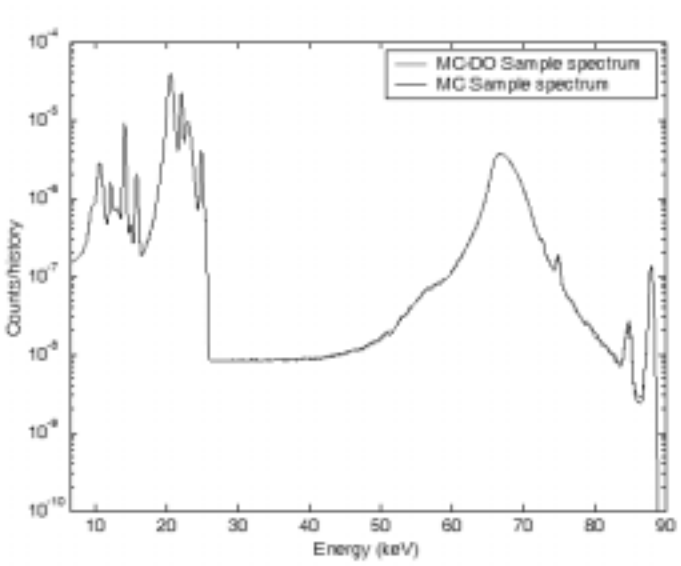

Figure 5.2 CEARXRF simulated sample spectrum for Case B compared with re-adjusted spectrum by applying Differential Operator to the sample spectrum of case A

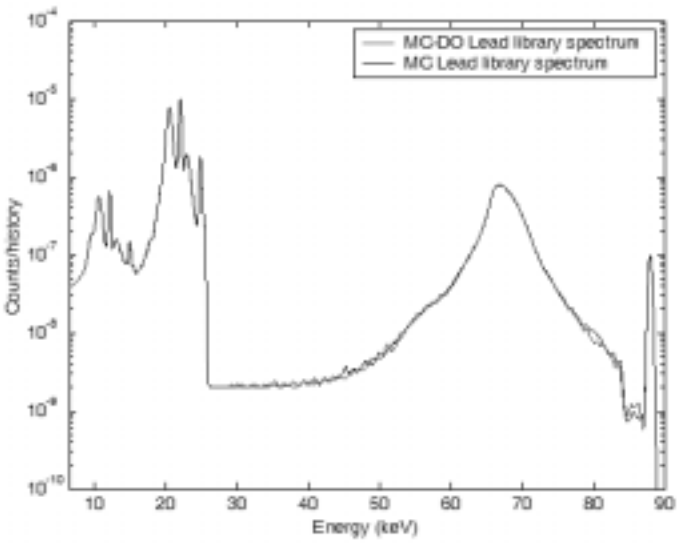

Figure 5.3 CEARXRF simulated Calcium library spectrum for Case B compared with the re-adjusted spectrum by applying Differential Operator to the Calcium library spectrum of case A

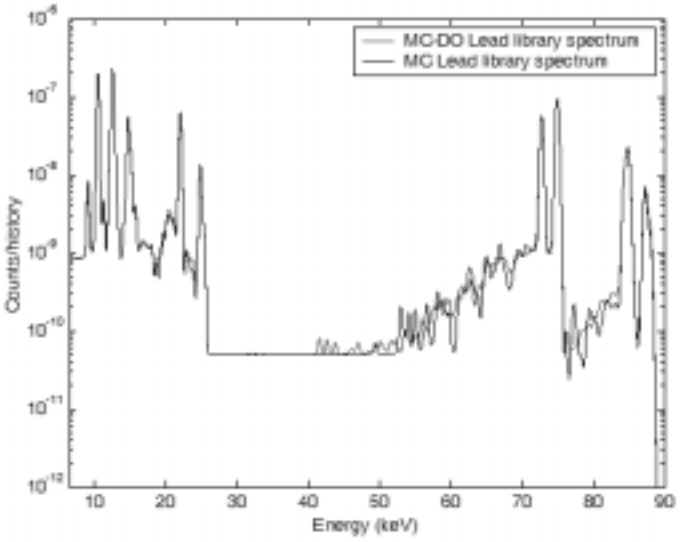

Figure 5.4 CEARXRF simulated Lead library spectrum for Case B compared with the re-adjusted spectrum by applying Differential Operator to the Lead library spectrum of case A

Table 5.3 MCDOLLS quantitative results by fitting sample spectrum of case B with re-adjusted elemental library spectra by applying Differential Operator to those of case A

Element	Calculated weight fraction (%)	True weight fraction (%)	Relative Error (%)
H	0.0206485	0.021849	5.49
C	0.00561796	0.004375	28.41
N	0.00263933	0.0020675	27.66
O	0.571180	0.554067	3.09
S	0.172637	0.174920	1.31
Ca	0.241050	0.241138	0.036
Sr	0.00141558	0.00141560	0.0014
Pb	0.000168024	0.000168	0.014

6. X-ray Coincidence Spectroscopy

6.1. Overview

The coincidence spectroscopy has been applied to various fields, such as radioisotope standardization (Martin and Taylor 1992; Taylor 1967) and gamma-gamma or particle-gamma coincidence measurements (Bartholomew et al. 1967; Hoogenboom 1958), to improve the measurement sensitivity and to better understand the physical process involved.

For the *in vivo* EDXRF measurement of lead in bone, the measurement sensitivity is limited by back-scattered source photons as discussed in section 1.3. Based on the true coincidence theory between K & L lines, the X-ray coincidence measurement is proposed and studied for the lead in bone application in this thesis. General advantages of coincidence spectroscopy to improve the measurement sensitivity are discussed further in the following.

The fundamental idea of coincidence spectroscopy is to detect multiple events that are correlated in occurrence time, with the background minimized at the same time. Suppose two detectors are available for the experiment, for events that are independent in occurrence time, the singles counting rate in two detectors are N_1 and N_2 respectively. For coincidence

measurement, a very short time window, τ (often in nanosecond or sub-nanosecond magnitude), is applied for the measurement. If two events, one from each detector, are detected within that time window, a coincidence event is scored. This is illustrated in figure 6.1, where only events of case A will be scored. Of all the coincidence events scored, there will be some events caused by the so-called chance coincidence. Mathematically, the chance coincidence events can be estimated with the following equation (Knoll 2000),

$$N_{chance} = \tau * N_1 * N_2$$

which shows that with the time window in 10^{-9} seconds order or less, the chance coincidence rate can be reduced greatly.

Those electronic instruments involved in this coincidence work can be classified into several categories.

1. Radiation detectors, e.g., solid state detectors and scintillation detectors
2. Analog energy pulse processing modules, e.g., photo-multiplier tubes, preamplifiers, linear amplifiers and timing filter amplifiers
3. Time pulse processing modules, e.g. constant fraction discriminators, coincidence units and timing to amplitude converters
4. Logic signal processing units, e.g. logic delay and gate modules

5. Analog to digital converters and memory units for data storage

Modules from category 1 through category 4 are of the NIM standard (NIM 1990). Modules in category 5 are of the CAMAC standard (Knoll 2000).

Due to the difficulty and significance of acquiring the logic time signal, timing technologies are reviewed in the next section. This is followed by experimental data and Monte Carlo coincidence simulation results.

6.2. Timing Technology

Theoretically, radiation detectors used by EDXRF applications can be considered as devices that transform the photon incidence event to an occurrence of current or voltage pulse (for sintillators, intermediate light pulses are generated too). The occurrence of a photon incidence event can be defined as the moment of the full/partial energy deposition in the detector (although multiple interactions might be involved in this process, but the time period is normally short enough to be ignored.). The occurrence time of the current or voltage pulse can be defined or picked with several techniques. The true photon incidence time is not directly measurable, so the timing mark is normally picked from the transformed current or voltage signal.

Before going further into the discussion of timing techniques, it is important to point out that there is always a delay between these two events due to various factors such as the charge collection time of the crystal, signal propagation delay and also delay of the intermediate instruments for cases where the pulse occurrence time is picked after some filtering or amplification. This difference of time is denoted as $\Delta T_{delay,inherent}$, which represents the time difference between the one obtained from the current or voltage pulse and the occurrence of the photon incidence event as shown in figure 6.2.

$\Delta T_{delay,inherent}$ is dominated by the inherent detector characteristics for fast timing applications. For the work of this thesis, two different types of detectors were used, the low energy Ge detector and the X-ray NaI(Tl) detector. For NaI(Tl) sintillators, the light signal transports very fast inside the crystal and the major component of $\Delta T_{delay,inherent}$ is caused by the propagation delay of the electron multiplication process (figure 6.3) in the photo multiplier tube, which is in the order of 10 ns (Knoll 2000). For germanium detectors, $\Delta T_{delay,inherent}$ is controlled by the charge collection process (figure 6.4), which can be estimated as 10ns / mm (Ortec 1999a). The technique to correctly adjust the extra delay for compensating the difference of $\Delta T_{delay,inherent}$ between different detectors will be discussed in the section of quality assurance.

Three different types of errors may affect the time resolution, namely, jitter, walk and drift (Knoll 2000; Ortec 1999b).

Time jitter is mainly caused by the electronic noise (figure 6.5), for the electronics noise causes uncertainty for the time at which the analog pulse crosses the discriminator threshold. If e_n is the voltage amplitude of the noise superimposed on the analog pulse, and dV/dt is the slope of the signal when its leading edge crosses the discriminator threshold, time jitter can be estimated as (Ortec 1999b):

$$\text{Time jitter} = e_n / (dV/dt).$$

It is clear that either by minimizing the signal noise or by increasing the slope of the leading edge (decreasing the rise time), the time jitter error can be reduced.

Time drift is a long-term behavioral phenomenon. It can be caused by thermal condition change or device aging. It is not quite often to be a problem with up-to-date electronics and has to be dealt with case by case if it occurs.

Time walk is the systematic dependence of the time marker on the amplitude or rise time of the input pulse (figure 6.6 and figure 6.7). The range of the pulse amplitude is dictated by

the energy range of interest in the application. The variation of rise time can be determined by the inherent features of the detector, such as for Germanium detector, the charge collection time difference due to different locations of the energy deposition inside the crystal can complicate this issue.

Two fairly good time pick-off techniques are the True Constant-Fraction timing (TCF) (Bedwell and Paulus 1976) and Amplitude and Rise Time Compensated timing (ARC) (Chase 1968). TCF picks time based on certain fraction of the incoming signal, so the amplitude walk can be minimized with the correct setting. The way it works is that for each input pulse, it will generate another signal by inverting and attenuating the input signal with a constant fraction. The summation of this inverted and attenuated signal and the delayed signal of the original input pulse forms a bipolar pulse. The time signal is obtained when the bipolar pulse crosses over the zero point, which is also exactly the time for the delayed signal to reach the constant fraction that was used to attenuate the inverted signal. The schematics of working principle of TCF are shown in figure 6.8. As also shown in figure 6.8, TCF minimizes the amplitude walk, but it still does not prevent the rise time walk. The ARC technique improves this aspect by reducing the amount of delay to generate the delayed signal, so the time mark is independent of both amplitude and rise time as shown in figure 6.9.

Also, during my experimental work, the slow rise time rejection feature is proven to be very helpful for improving the time resolution.

6.3. Time Spectrum Measurement for Quality Assurance

The quality of electronics settings for time pick-off can be assured with the time spectrum measurement. The schematic of electronics connection is presented in figure 6.10.

Measurements were made for two different detector combinations. The first combination used two X-ray NaI(Tl) detectors. Each detector had a Be window and NaI(Tl) crystal of 1mm thickness and 50.8mm diameter. The second combination used a low energy Germanium detector and a X-ray NaI(Tl) detector. Measured time spectra for both combinations are shown in figure 6.11 and figure 6.12 respectively.

Two parameters from the time spectrum are very important for electronics setting of coincidence measurements. The first is the centroid value of the time peak, which is used to set the extra delay unit for compensating the difference of the $\Delta T_{delay,inherent}$ between different types of detectors. For the Germanium and NaI(Tl) combination, the NaI(Tl) loop signal should be delayed for about 150ns. The second parameter is the Full Width Half Maximum (FWHM) of the time peak, which is used for setting the window width of coincidence units.

From figures 6.11 and 612, it is clear that the combination of same type of detectors gives better timing resolution, about 20ns (FWHM of the time peak). The Germanium and NaI(Tl) pair has timing resolution of about 200ns, which is good enough for the counting rates of our application (10^5 s^{-1}).

6.4. Electronics and Setting Procedures

The schematic of electronics connection for coincidence measurement is shown in figure 6.13. NIM modules (NIM 1990) are used for the analog pulse processing. CAMAC (Knoll 2000) ADCs and memories are used for fast data communication with PC. The data acquisition software used was KMAX 7 by SPARROW Corp. CEARCOINC.tlsh was developed as the data acquisition toolsheet (figure 6.14), by which the data acquisition information can be stored and the process can be controlled. One very nice feature of the system is that just by running the experiment once, three sets of data are available for further analysis, which include singles spectra, coincidence spectra and multi-dimensional coincidence data.

Compared to the singles experiment of the EDXRF measurement, electronics settings are much more complicated, since time calibration is involved in addition to energy calibration. After a lot of “trial and error” work, a systematic electronics setting procedure is formulated

as following:

1. Circuit connection (figure 6.13) with power off
2. Power on and apply high voltage to detectors (caution: correctness of connection)
3. Refer to detector manuals, set the linear amplifiers' shaping time constant
4. Set the linear amplifier gain for each loop by energy calibration
5. Estimate the pulse height range of linear amplifier outputs according to the energy range under investigation (caution: linearity of those modules involved needs to be assured)
6. For each loop, connect the linear amplifier output, timing filter output (duplicated from the input of CFD to make sure the 50 ohm resistance), and CFD output at the same time to a oscilloscope, make sure each of the linear amplifier output pulses with heights in the specified range above can be accompanied with a valid CFD time pulse output. Factors to adjust:
    - Timing filter gain
    - Timing filter differentiation constant
    - Timing filter integration constant
    - CFD threshold (CFD output trigger time)
    - CFD delay (40% rise time)
    - CFD mode (SR CF)
    - CFD time walk

7. Time spectrum measurement to assure CFD outputs for coincidence events are triggered at the same time, i.e., $\Delta T_{delay,inherent}$ is compensated correctly
8. Set the coincidence unit resolving window equal to the FWHM of the time peak from step 7
9. Observe the gate signal and two linear amplifier signals together on the oscilloscope to make sure that the gate is triggered at least 500ns before the pulse peak is reached and the width of the gate extends 500ns after the peak. (Figure 6.15). This time synchronization is as required by the CAMAC ADC used.
10. Start measurement with CEARCOINC.tlsh

6.5. Experimental Results

For the X-ray coincidence study, several experiments were conducted, with different combinations of detectors and for different purposes.

To experimentally verify the true coincidence theory of K and L lines, one pure Lead sample was studied with a collimated Cd-109 radioisotope source and two different combinations of detectors. One pair of X-ray NaI(Tl) detectors are used for one experiment for simplicity of the timing adjustment, and the low energy Germanium detector substituted one of them in the other experiment for better energy resolution. The X-ray NaI(Tl) detector

has a NaI(Tl) crystal with thickness of 1mm and diameter of 50.8mm. The entrance window is made of Be with 0.1mm thickness.

Experimental results with two NaI(Tl) detectors are shown in figure 6.16 and figure 6.17. From the singles and coincidence spectra comparison of figure 6.16, it is clear that those peaks of back-scattered source photons (88.0 keV Cd-109 γ ray and 22.2 keV, 24.9 keV Ag X rays) are minimized or eliminated in the coincidence spectrum. Those peaks in the coincidence spectrum can be better explained with the assistance of 2-D scatter plot of figure 6.17, which is very informative since it expresses the energy pair information for coincidence events. Obviously, the K and L X-ray coincidences are observed by the experiment and also L and L coincidence events. The reason for L and L coincidence is that the K X ray from one atom can excite the L X ray of another atom. Then the L X ray in coincidence with the K X ray in the original atom is also in coincidence with the L X ray produced by the interaction of the K X ray in the other atom. The intensity of L and L coincidence events are higher than expected. This is possibly related to the rough surface of the lead sample for the measurement. Also cross talk events are seen in the coincidence spectrum, which means the iodine X ray activated in detector 1 is detected by detector 2, in coincidence with the escape peak of detector 1, and vice versa. Note that the L-L coincidence events are proportional to the lead content, but the cross talk coincidence events are not. The L-L coincidence events will probably have a slightly different spatial distribution from that of the K-L coincidence

events.

Experimental results with LEGe and X-ray NaI(Tl) detectors are shown from figure 6.18 to figure 6.20. One improvement compared to the previous experiment is that the better resolution of the LEGe detector makes the lines with close energy values resolvable. The same explanation for the previous experiment is also applicable here.

With these two experiments, the coincidence measurement is proved to be effective for minimizing the detection of back-scattered source photons, which are not in true coincidence with other photons. However, it is also noted that counting rates for lead K and L lines are also reduced by almost three orders of magnitude. This is caused by several factors including: fluorescence yield of the L shell, detector solid angle, and attenuation within the sample itself. This reduction has a negative effect on obtaining good statistics of the K and L lines. For pure lead, this is not a big problem because of rather high counting rates of these lines. But for the bone sample, with trace amount of lead, this reduction causes problem for the same spectrometers used for pure lead measurement.

Based on this observation, a prototype of X-ray coincidence spectrometer is proposed as in figure 6.21. The low energy Ge detector is surrounded with a big and thin NaI(Tl) detector to increase the detection efficiency without introducing significant amount of noise. The

advantage of this spectrometer is to combine the good resolution of Ge detectors and the high efficiency of NaI(Tl) scintillators with big surface area. The CEARXRF was benchmarked with pure lead measurement data for the coincidence simulation capability in section 6.6 and simulated results for this prototype spectrometer are presented in section 6.7.

6.6. Monte Carlo Coincidence Simulation and Benchmark Results

To further investigate and optimize X-ray coincidence spectrometers, the Monte Carlo simulation code CEARXRF was updated to simulate the coincidence events.

The measurement with low energy Ge detector and X-ray NaI(Tl) detector was used to benchmark the coincidence simulation of CEARXRF. The modeled geometry is shown in figure 6.22.

The simulated singles spectrum of the low energy Ge detector is compared with the experimental spectrum in figure 6.23, which shows good agreement. Some discrepancies in the Compton continuum are possibly due to the error of geometry modeling.

In figure 6.24, the simulated coincidence spectrum is compared with the experimental coincidence spectrum of the low energy Ge detector. Several peaks in the experimental

coincidence spectrum does not show up in the simulated one, since they are caused by the cross talk effect (Iodine X Ray from the NaI(Tl) detector) and CEARXRF can not simulate this effect at the present time. As far as the K coincidence peak, it is a good fit. The discrepancy for L lines are possibly caused by two reasons:

- Rough surface of the lead sample under measurement makes the attenuation of the sample to L lines weaker than that from a ideal sample of smooth surface
- Ge escape peaks of Ag X rays in coincidence with detection of Ge characteristic X rays in the NaI(Tl) detector, which have close energy value as that of Pb L X rays

To make a better comparison between the simulation and experiment, a diagonal energy window was applied to the 2-d scatter measurement data to generate the coincidence spectrum, which is more physically close to simulation conditions. The comparison is presented in figure 6.25. It is clear that they fit with each other very well.

6.7. Monte Carlo Coincidence Simulation with the Proposed X-ray Coincidence Spectrometer

By Monte Carlo coincidence simulation, the proposed X-ray coincidence spectrometer (figure 6.21) was compared with the present spectrometer used for the previous experiment (low energy Ge detector and small NaI(Tl) detector) for lead in bone measurement.

The modeled geometries for the Monte Carlo simulation are in figure 6.26 and figure 6.27 respectively. Simulated coincidence spectra for two cases are compared in figure 6.28. It is clear that the proposed X-ray coincidence spectrometer can improve the detection efficiency with almost one order of magnitude, which is enough to obtain good statistics for lead K and L x-rays to make quantitative determination of lead composition of human bones.

6.8. MCLLS Application to Coincidence Study for Lead Determination

To apply the MCLLS method to coincidence study for lead determination, two calculation cases were made.

The first study was based on the pure lead measurement with the coincidence spectrometer (LEGe and 2" NaI X-ray detector) available. For this study, the total experimental coincidence spectrum in figure 6.24 was taken as the unknown and the diagonal summing spectrum, figure 6.25, was taken as the lead only library spectrum. The difference between the total spectrum and the lead library was considered to be the background spectrum. The fitted Chi-squares value is 1.63 and the lead amount is $0.96 \pm 1.99\%$.

The second study worked on the simulated coincidence spectrum by the proposed X-ray coincidence spectrometer. In the simulated spectrum, the diagonal summing data (figure 6.28)

was treated as the total spectrum. Lead was considered to be the only element that can contribute in that region except chance coincidence background. The fitted Chi-squares value is 0.98 and the lead amount is 162ppm $\pm$ 0.1%.

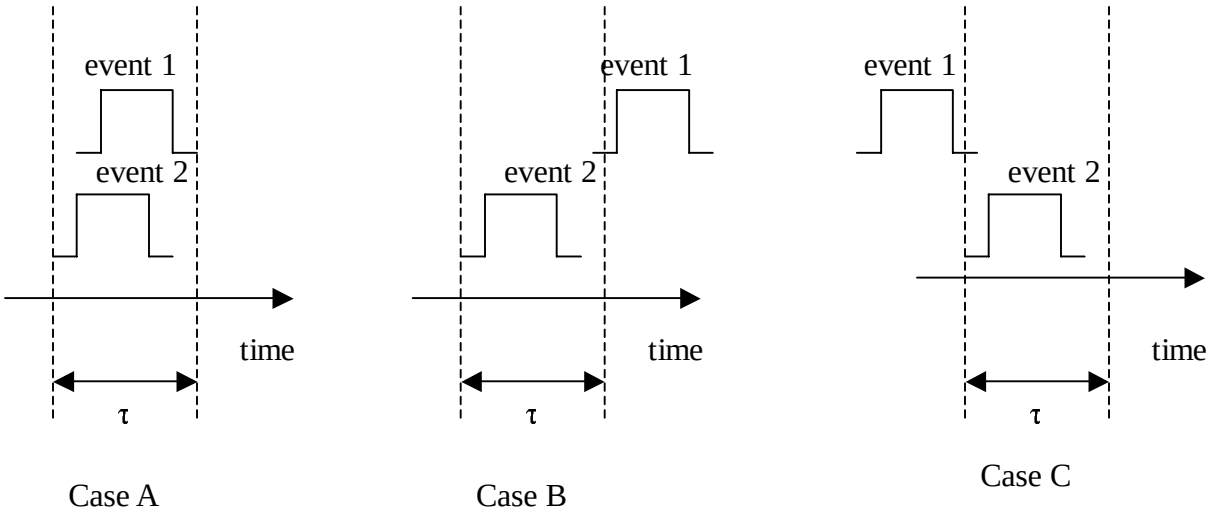

Figure 6.1 Schematics of correlated and uncorrelated pulses in time

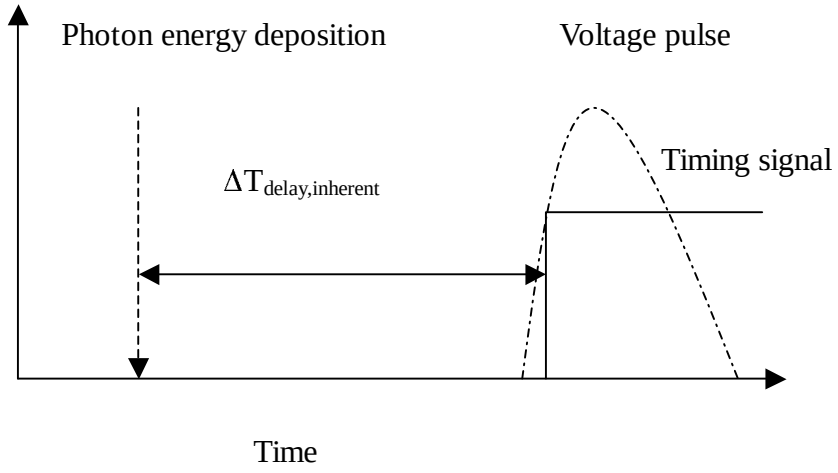

Figure 6.2 Schematics of $\Delta T_{delay,inherent}$, the systematic error of occurrence time measurement for photon incidence events

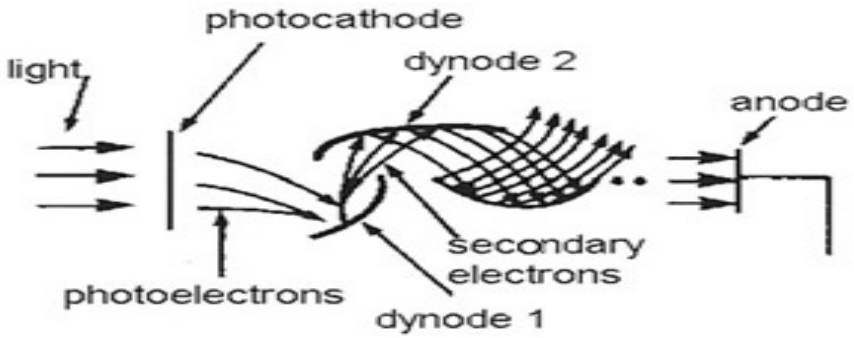

Figure 6.3 Schematics of linearly focused photo multiplier tube structure

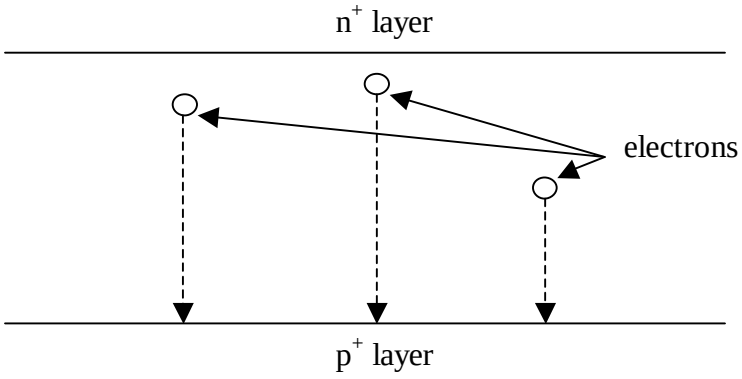

Figure 6.4 Electron drifting process in the Germanium crystal

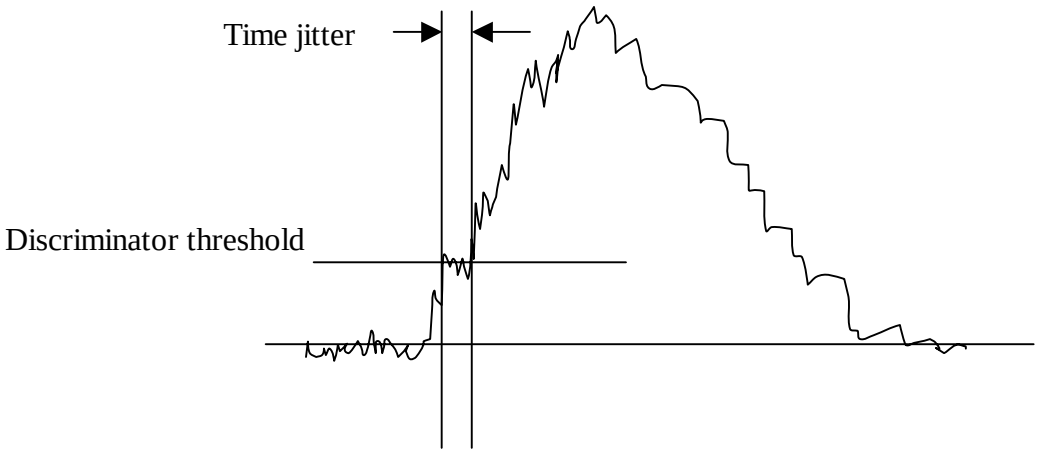

Figure 6.5 Schematics of time jitter caused by electronic noises superimposed on incoming pulses

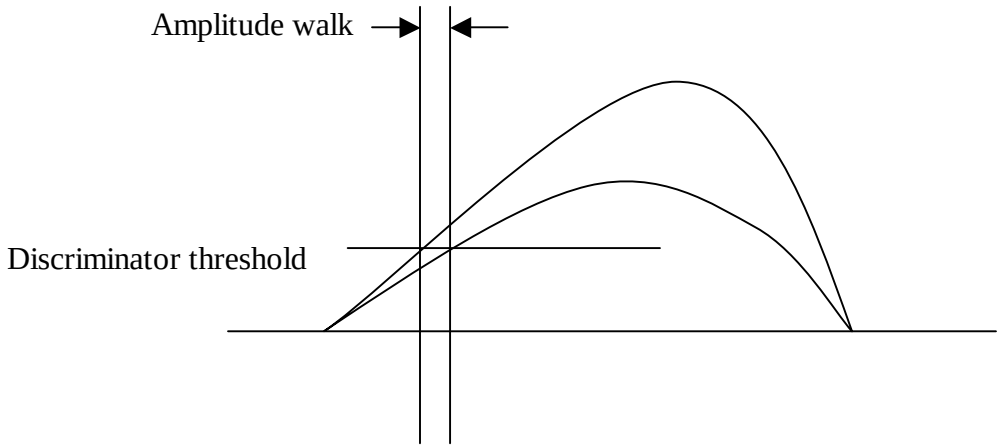

Figure 6.6 Schematics of time walk caused by pulse amplitude variation

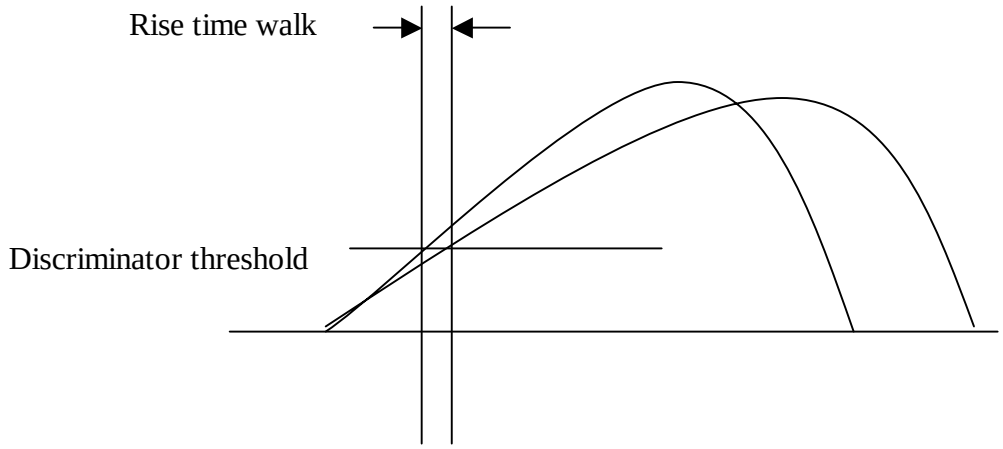

Figure 6.7 Schematics of time walk caused by pulse rise time variation

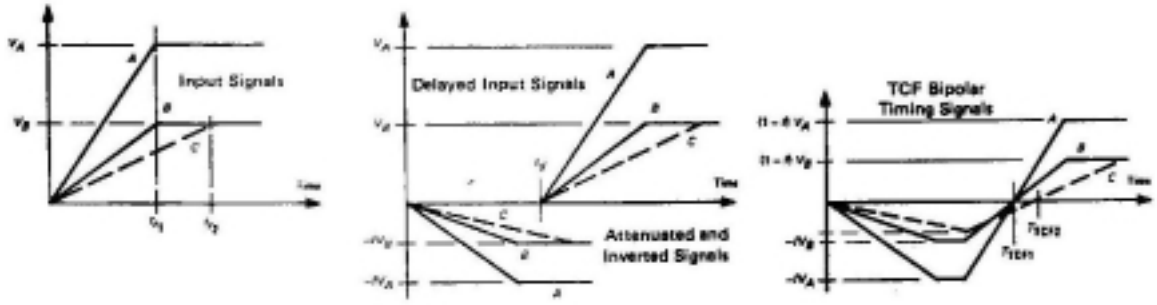

Figure 6.8 Working principle of the true constant fraction (TCF) technique to pick off time

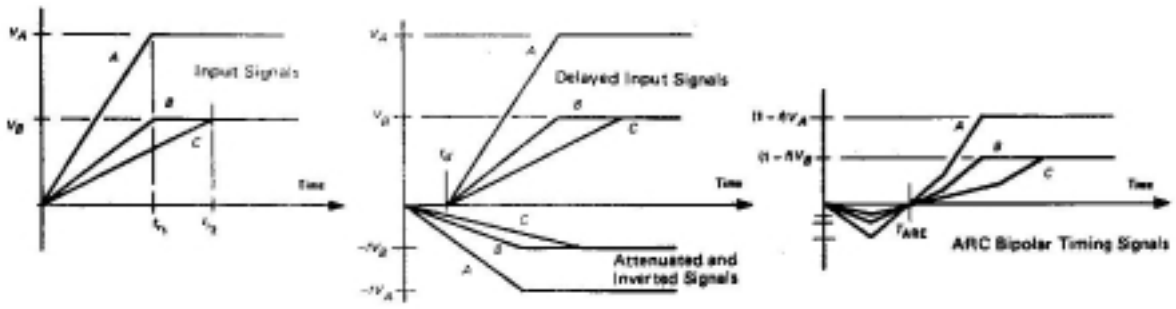

Figure 6.9 Working principle of the amplitude and rise time compensated (ARC) technique to pick off time

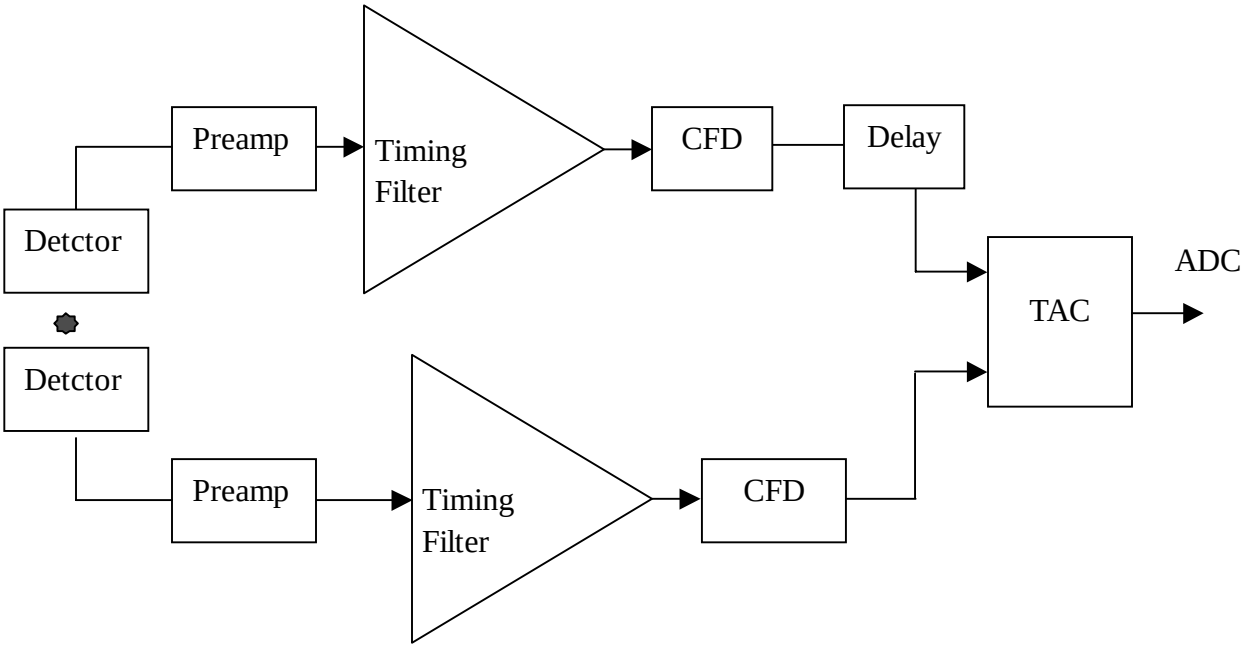

Figure 6.10 Schematic of electronics connection for time spectrum measurement

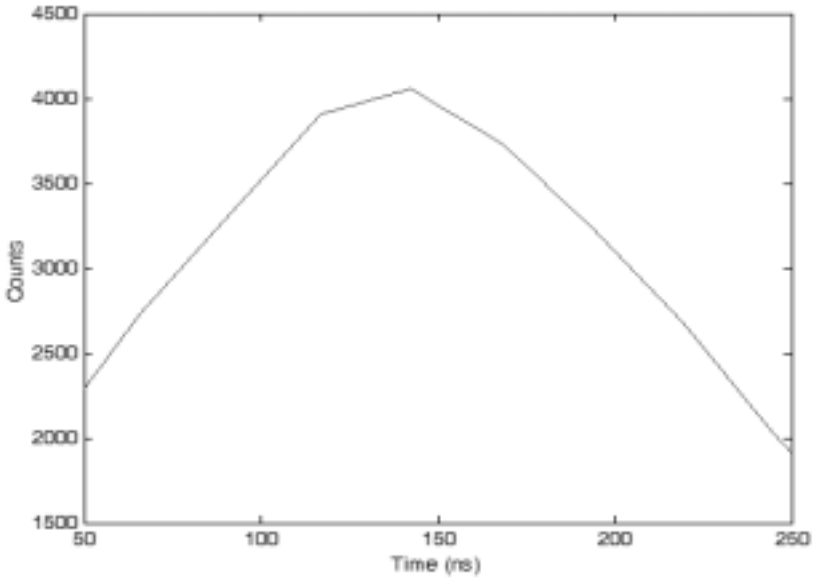

Figure 6.11 Experimental time spectrum with LEGe & X-ray NaI(Tl) detectors

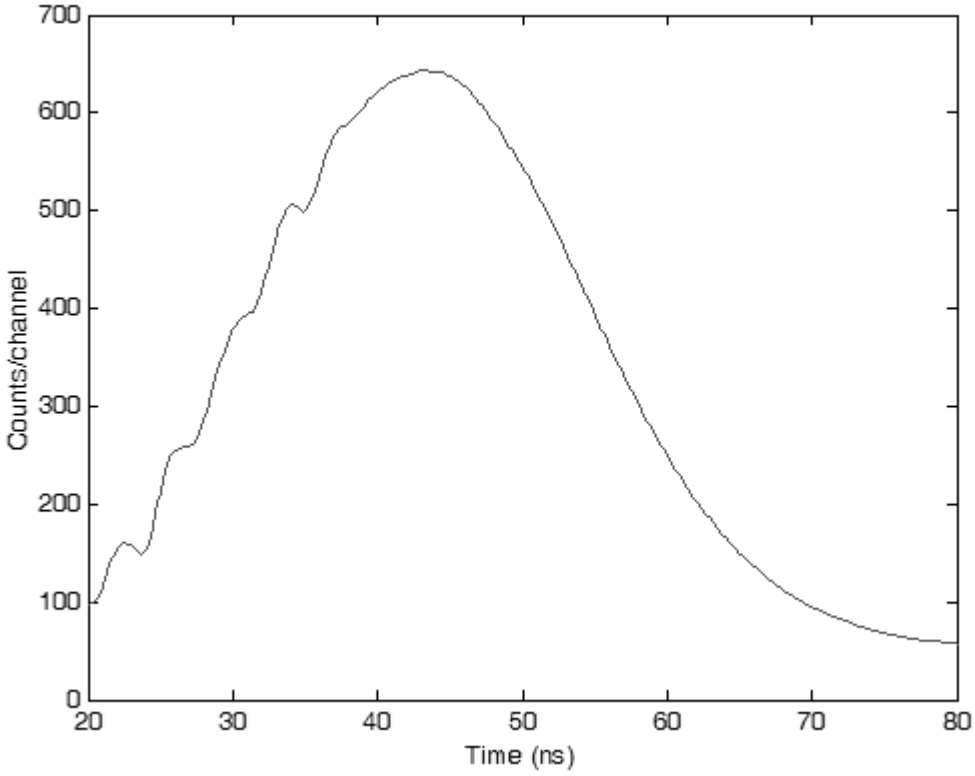

Figure 6.12 Experimental time spectrum with two X-ray NaI(Tl) detectors

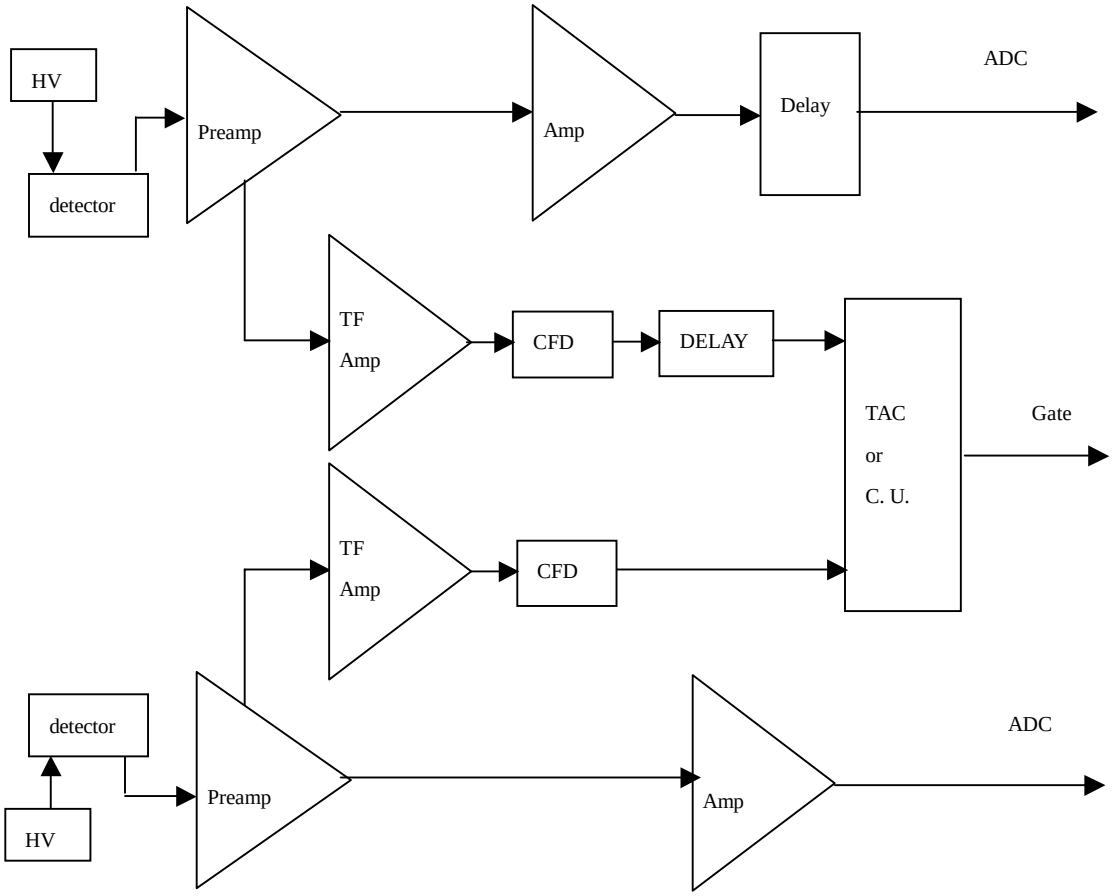

Figure 6.13 Schematics of electronics connection for two-parameter coincidence measurement

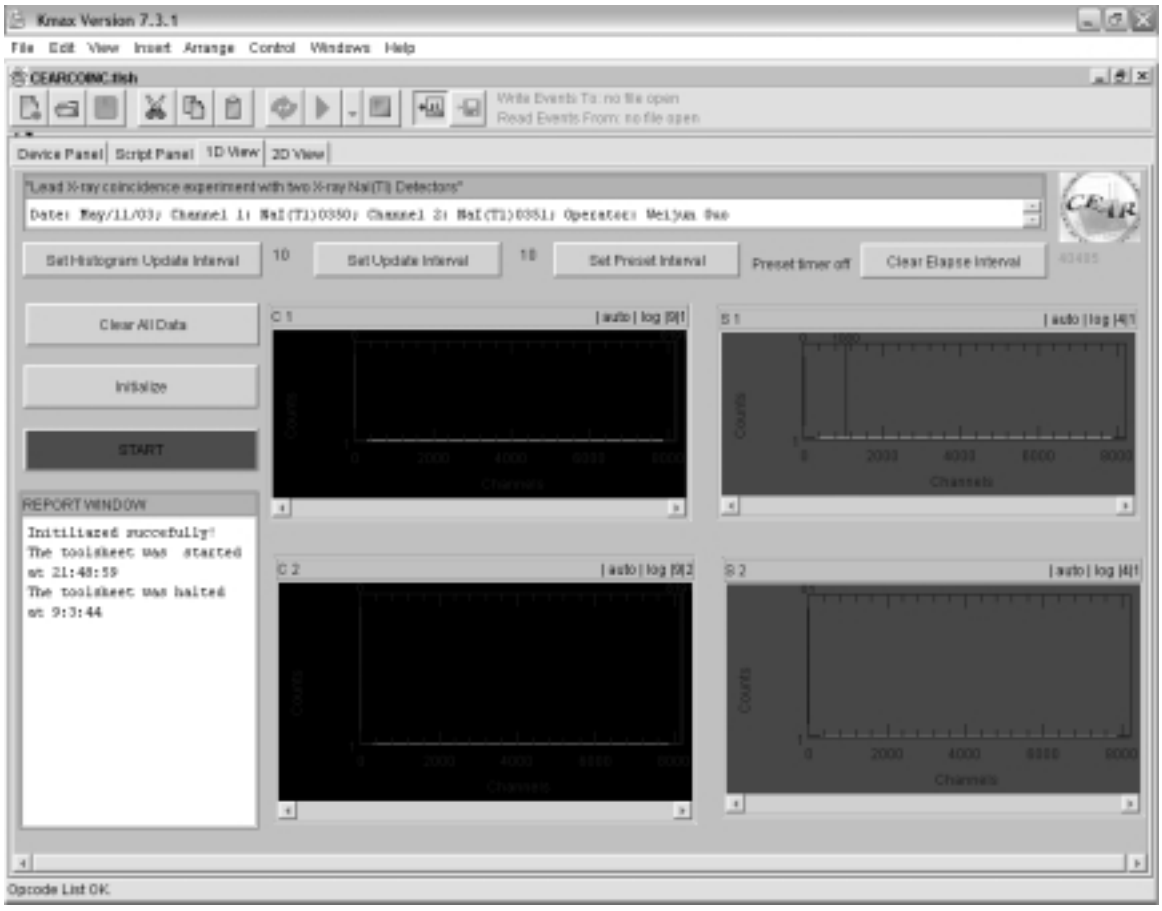

Figure 6.14 Screen shot of the Kamx 7 data acquisition toolsheet CEARCOINC.tlsh

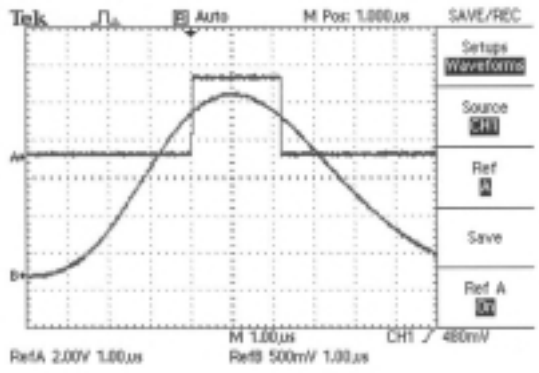

Figure 6.15 Oscilloscope screen printout to show the timing synchronization between the coincidence gate signal and the ADC input pulse

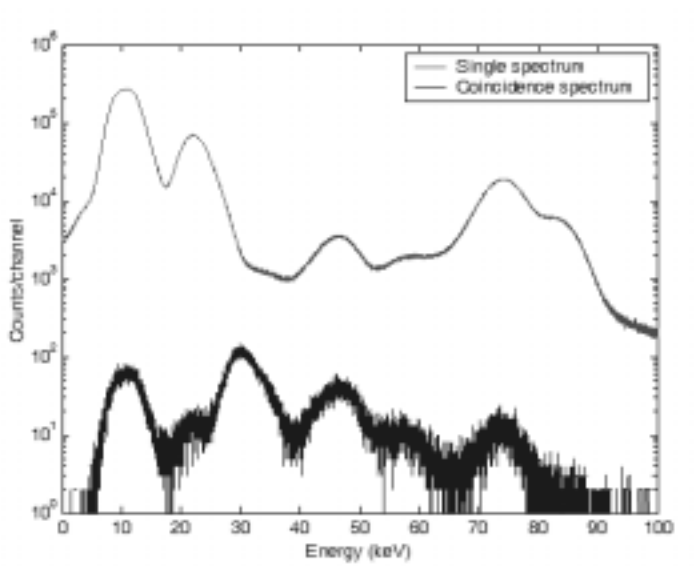

Figure 6.16 Experimental singles and coincidence spectrum for pure lead measurement with two X-ray NaI(Tl) detectors

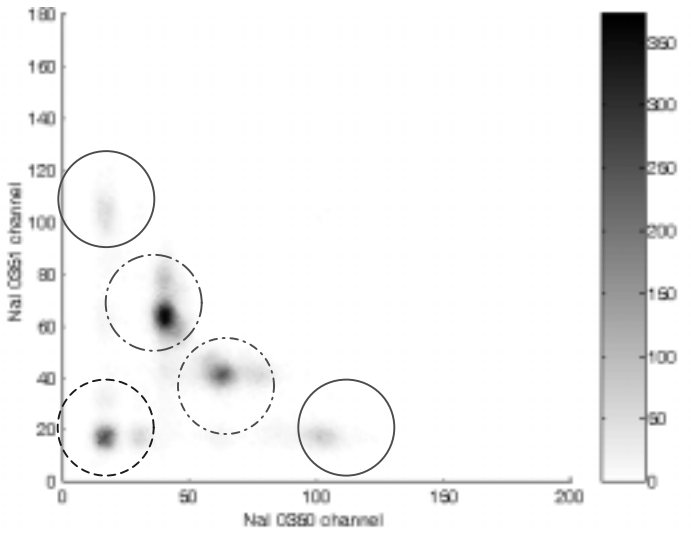

K & L Coincidence L & L Coincidence Cross talk effect

Figure 6.17 2-D scatter plot for experimental data of pure lead measurement with two X-ray NaI(Tl) detectors

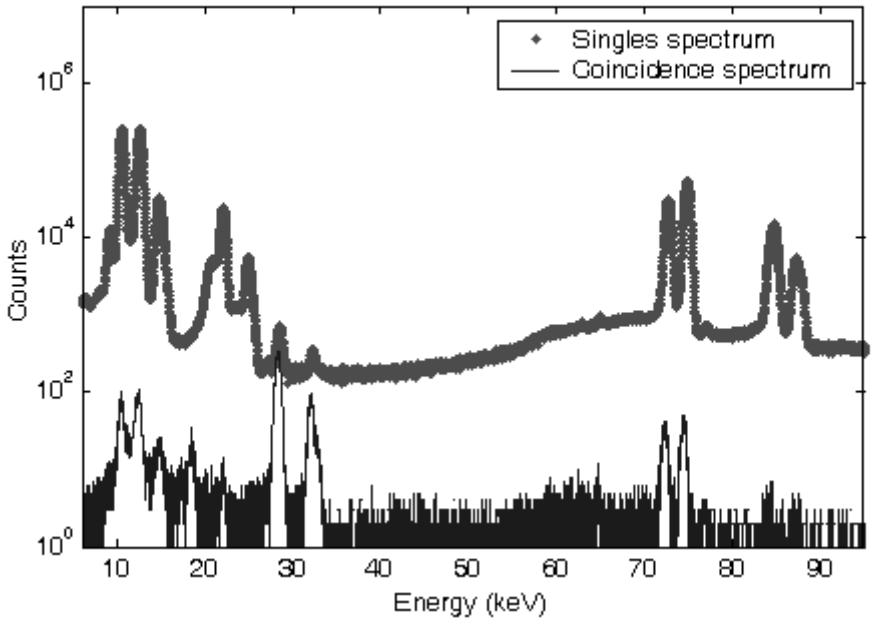

Figure 6.18 Experimental singles and coincidence sepectra for pure lead measurement with Ge detector

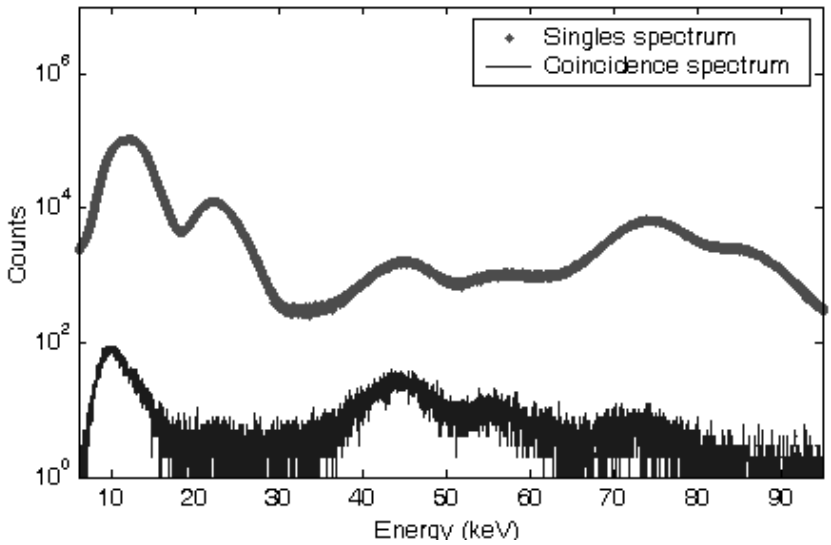

Figure 6.19 Experimental singles and coincidence spectra for pure lead measurement with X-ray NaI(Tl) detector

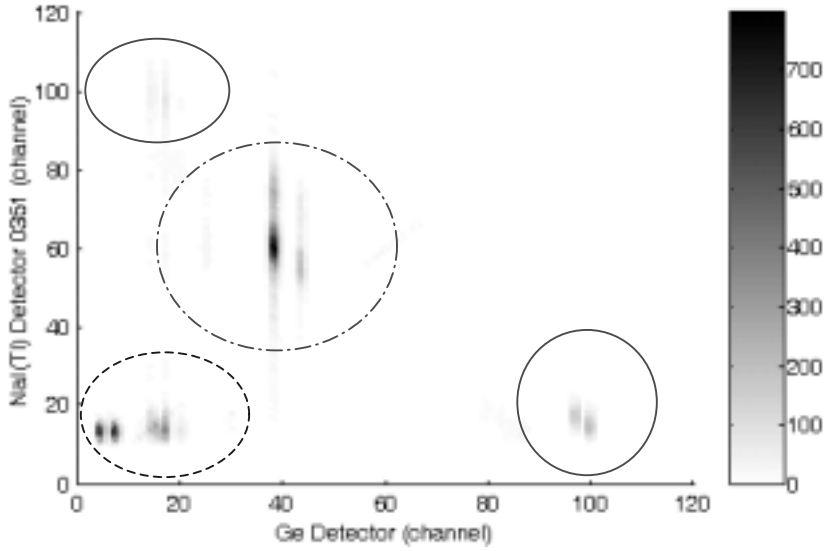

○ K & L Coincidence ◌ L & L Coincidence + cross talk ◌ Cross talk effect

Figure 6.20 2-D scatter plot for experimental data of pure lead measurement with NaI(Tl) detector and low energy Ge detector

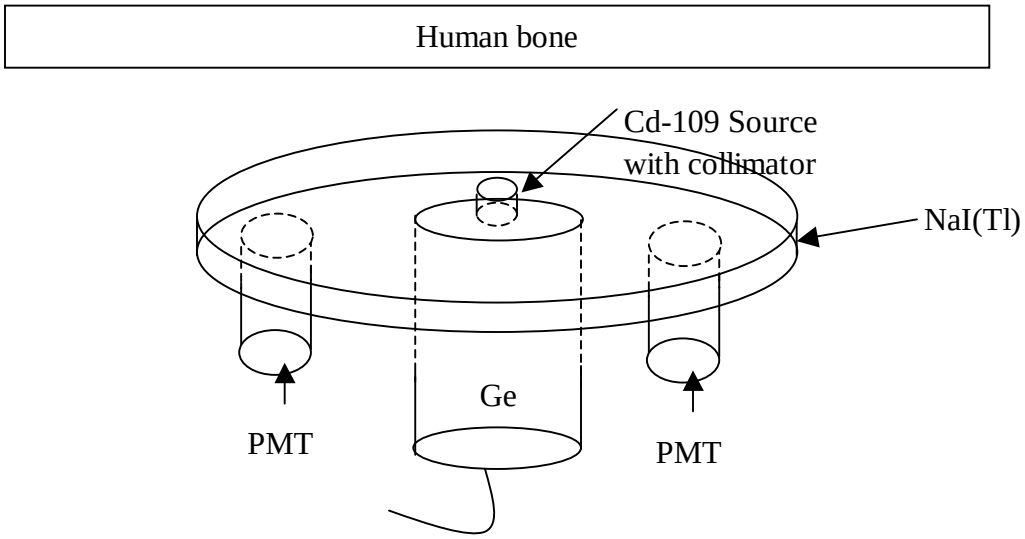

Figure 6.21 Proposed X-ray coincidence spectrometer for *in vivo* lead in bone measurement with low energy Ge and customized X-ray NaI(Tl) detectors

Figure 6.22 Geometry for benchmarking Monte Carlo coincidence simulation

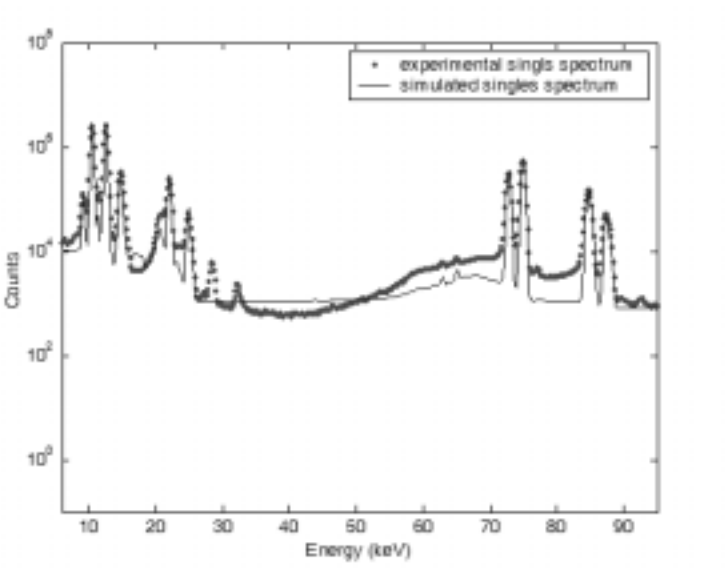

Figure 6.23 CEARXRF simulated singls spectrum compared with the measured singles spectrum with Ge detector

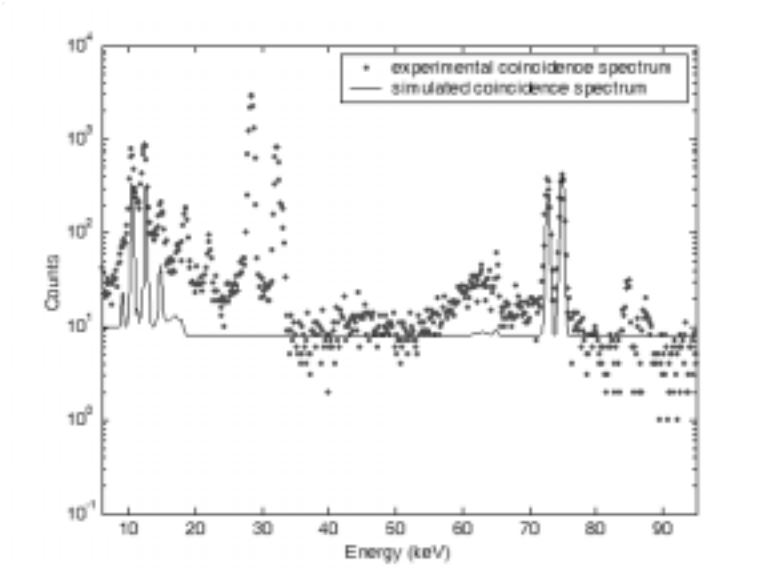

Figure 6.24 CEARXRF simulated coincidence spectrum compared with the measured coincidence spectrum with Ge detector

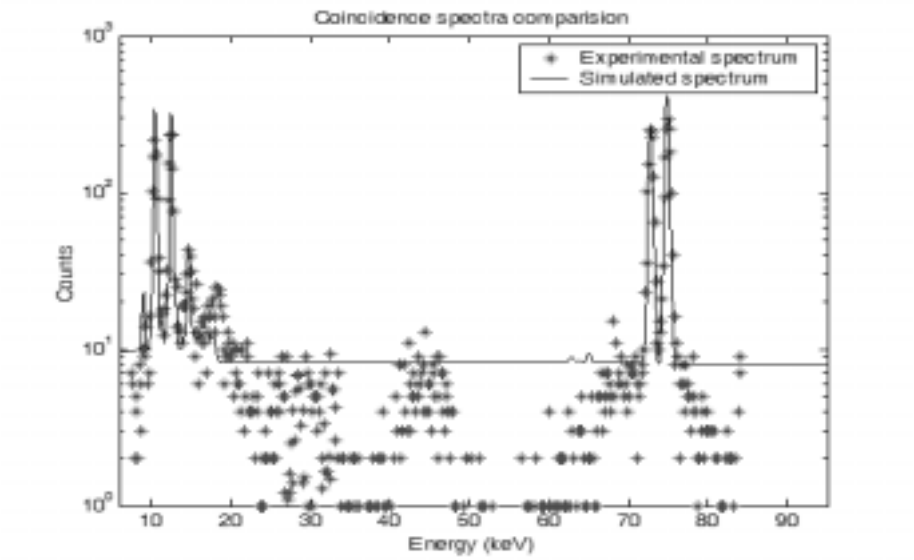

Figure 6.25 CEARXRF simulated coincidence spectrum compared with the experimental diagonal summing coincidence spectrum

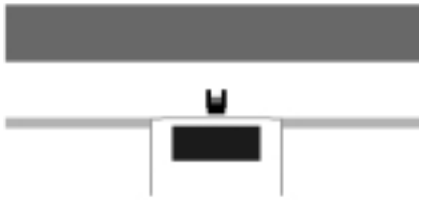

Figure 6.26 Geometry plot for X-ray coincidence measurement of lead in bone with the proposed X-ray coincidence spectrometer

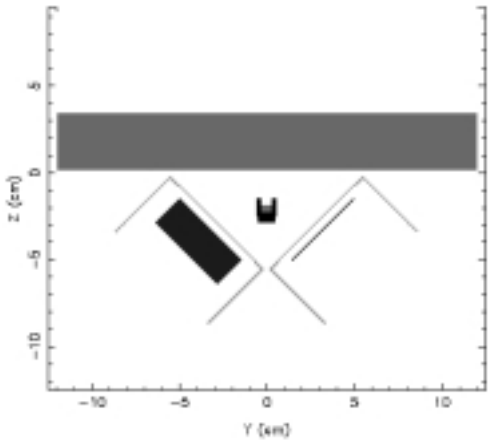

Figure 6.27 Geometry plot for X-ray coincidence measurement of lead in bone with the small X-ray NaI(Tl) detector and the low energy Ge detector

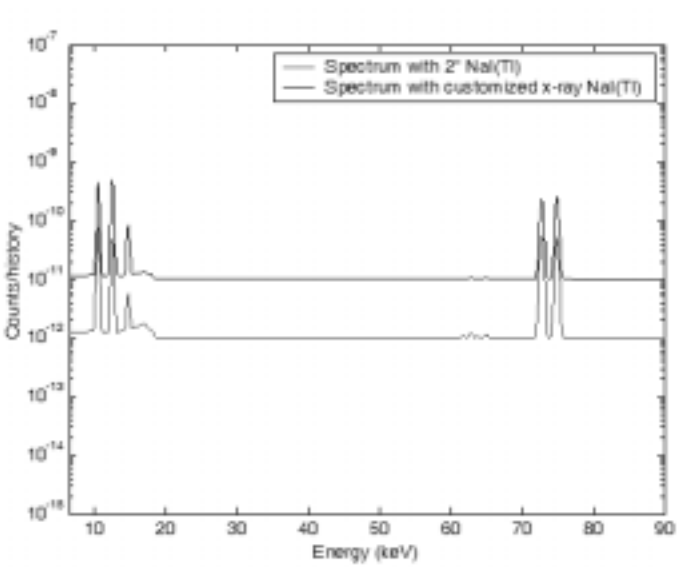

Figure 6.28 X-ray coincidence spectra comparison for lead in bone measurement

7. Conclusions and Discussion

The Monte Carlo simulation code CEARXRF was updated to apply the MCLLS method for *in vivo* lead in bone EDXRF measurement.

The bone sample of Plaster of Paris with 162ppm of lead was measured with the low energy Ge spectrometer and Cd-109 radioisotope source to benchmark the simulation (figure 2.2). The simulated sample spectrum shows good agreement with the experimental sample spectrum (figure 2.3). This validates the idea of using Monte Carlo simulation for the optimization of the spectrometer, since the simulated sample spectra can be studied as good approximations of experimental sample spectra for various conditions.

The elemental library spectra simulated with CEARXRF were used to fit the experimental sample spectrum to quantitatively determine the lead composition of the bone sample. The determined value (table 3.2) is accurate compared to the certified value.

The Monte Carlo - Differential Operator method was implemented in CEARXRF for quantitative matrix effect and measurement sensitivity study by simulating differential responses of elemental library spectra to variations of elemental compositions. Simulated

differential responses are explained in chapter 4.

The MCLLS method was successfully combined with the Differential Operator method, MCDOLLS. Two bone samples with different lead compositions were simulated with CEARXRF. The quantitative lead determination results with different library spectra sets are compared (table 5.2 and table 5.3), which show the improvement of the MCDOLLS method over the MCLLS method for lead in bone measurement.

X-ray coincidence spectroscopy was proposed in this thesis, which is promising to improve the measurement sensitivity of EDXRF measurement.

Time spectra were measured for coincidence measurements for quality assurance purpose (figure 6.11 and figure 6.12). A complete procedure for setting the electronics for the coincidence measurement is presented in section 6.4.

Two coincidence experiments with different detectors combination were done to verify the X-ray coincidence physics (figure 6.16 to figure 6.20). The experimental data were further used to benchmark the implemented x-ray coincidence simulation capability of CEARXRF (figure 6.23 and figure 6.25), which show good agreement with each other.

To apply the X-ray coincidence spectroscopy to trace level bone lead measurement, a customized coincidence spectrometer (figure 6.21) was proposed and was simulated with the Monte Carlo code CEARXRF. The advantage of this spectrometer is to combine the high efficiency and low cost feature of big X-ray NaI(Tl) detectors with the fine energy resolution of low energy Ge detectors. The detection efficiency was proved to be one magnitude higher than the current spectrometer we used for benchmarking the CEARXRF coincidence simulation.

8. Future Work

It is more and more recognized that the Monte Carlo simulation is a very important methodology to possibly substitute experimental studies. The random number generator is a key component for the success and reliability of the Monte Carlo simulation. The effects of different random number generators on simulation may be investigated quantitatively and indicators of goodness of random number generators may be formulated.

The MCLLS method to determine elemental compositions is powerful and convenient to use in the sense of accuracy and error analysis. It is good to extensively study the effects of the following on fit results:

- Different element combinations (such as some elements with very close library spectra)
- Erroneous or incomplete information of chemical elements of the unknown sample (systematic procedure to make correction)
- Statistics of library spectra and variable weighting for different channels
- Fitting algorithms (direct solver v.s. iterative solver)

The MCDOLLS method is a promising method. The application of it to cases where on

line measurement is required can be effective. More benchmark cases are necessary to make it generally applicable. A good benchmark case may be an extensive study of series of alloy samples from NIST.

The X-ray coincidence measurement can be more effective for cases where minor or major elements need to be measured. With commercially available detectors (lowest measurable energy around several hundred electron volts), elements measurable can be from Titanium to Uranium.

References

Ao, Q., and Gardner, R. P. (1995). "The McLDL Code with Subspace Weight Window Biasing Combined with the Monte Carlo Multiply Scattered Components Approach for Simulation of Gamma-Gamma Lithodensity Logging Tools." *International journal of radiation applications and instrumentation. Part E, Nuclear geophysics*, 9(6), pp. 497-515.

Ao, Q., Lee, S. H., and Gardner, R. P. "Accuracy Evaluation of K and L XRF Lead in Bone (Tibia) Measurement by simulation with the Specific Purpose Monte Carlo Code NCSXRF." *IEEE 1995 Nuclear Science Symposium*, San Francisco, CA, 21-28.

Ao, Q., Lee, S. H., and Gardner, R. P. (1997a). "Development of the Specific Purpose Monte Carlo Code CEARXRF for the Design and Use of *In Vivo* X-ray Fluorescence Analysis Systems for Lead in Bone." *Applied Radiation and Isotopes*, 48(10-12), pp. 1403-1412.

Ao, Q., Lee, S. H., and Gardner, R. P. (1997b). "Optimization of *in vivo* X-ray Fluorescence Analysis Methods for Bone Lead by Simulation with the Monte Carlo Code CEARXRF." *Applied Radiation and Isotopes*, 48(10-12), pp. 1413-1423.

Ao, Q., Lee, S. H., and Gardner, R. P. "Applications of the Monte Carlo - Library Least-Squares *In Vivo* XRF Measurement of Lead in Bone." *Denver X-Ray Conference*, ICDD, Newtown Square, PA, 922-931.

Ao, Q., Lee, S. H., and Gardner, R. P. (1999b). "Error Analysis of the *In Vivo* XRF Measurement of Lead in Bone by Monte Carlo Simulation." *Advances in X-ray Analysis*, 41, pp. 898-909.

Arinc, F., Gardner, R. P., Wielopolski, L., and Stiles, A. R. (1975). "Applications of the least-squares method to the analysis of XRF spectral intensities from atmospheric particulates collected on filters." *Advances in X-ray Analysis*, 19, pp. 367-380.

Barry, P. (1975). "A comparison of concentrations of lead in human tissues." *British journal of applied physics*, 32, pp. 119-139.

Barry, P. (1981). "Concentrations of lead in the tissues of children." *British journal of applied physics*, 38, pp. 61-71.

Barry, P., and Mossmann, D. (1970). "Lead concentrations in human tissues." *British journal of industrial medicine*, 27, pp. 339-351.

Bartholomew, G. A., Naqvi, S. I. H., Gunye, M. R., and Earle, E. D. (1967). "The $^{199}Hg(n,\gamma)^{200}Hg$ reaction with thermal neutrons." *Canadian Journal of Physics*, 45, pp. 1517-1540.

Bearden, J. A., and Burr, A. F. (1967). "Reevaluation of X-ray Atomic Energy Levels." *Reviews of Modern Physics*, 39(1), pp. 125-142.

Bedwell, M. O., and Paulus, T. J. (1976). "A new Constant Fraction Timing System With Improved Time Derivation Characteristics." *IEEE transactions on nuclear science*, NS-23(1), pp. 234-243.

Bertin, E. P. (1978). *Introduction to X-ray spectrometric analysis*, Plenum Press, New York.

Biggs, F., Mendelsohn, L. B., and Mann, J. B. (1975). "Hartree-Fork Compton Profiles for the Elements." *Atomic Data and Nuclear Data Tables*, 16, pp. 201-310.

Briesmeister, J. F. (1997). "MCNP - A General Monte Carlo N-Particle Transport Code, Version 4B." *LA-12625-M*, Los Alamos National Labotary.

Briesmeister, J. F. (2000). "MCNP - A General Monte Carlo N-Particle Transport Code, Version 4C." *LA-12625-M*, Los Alamos National Labotary.

Carter, L. L., and Cashwell, E. D. (1975). *Particle-transport simulation with the Monte Carlo method : prepared for the Division of Military Application, U. S. Energy Research and Development Administration*, Technical Information Center Office of Public Affairs U. S. Energy Research and Development Administration, Springfield, Va.

Cashwell, E. D., and Everett, C. J. (1959). *A practical manual on the Monte Carlo method for random walk problems*, Pergamon Press, New York,.

Chase, R. L. (1968). "Pulse Timing System for Use with Gamma Rays on Ge(Li) Detectors." *The Review of Scientific Instruments*, 39(9), pp. 1318-1326.

Chettle, D. R., Scott, M., and Somervaille, L. (1991). "Lead in bone: Sampling and quantitation using K X-rays excited by Cd109." *Environmental health perspectives*, 91, pp. 49-55.

Criss, J. W., and Birks, L. S. (1968). "Calculation Methods for Fluorescence X-Ray Spectrometry Empirical Coefficients vs. Fundamental Parameters." *Analytical Chemistry*, 40, pp. 1080-1086.

Everett, C. J., and Cashwell, E. D. (1973). "MCP code Fluorescence-Routine Revision." *LA-5240-MS*, Los Alamos Scientific Laboratory, Los Alamos, New Mexico 87544.

Gardner, R. P., Mickael, M. W., and Verghese, K. (1989). "Complete composition and density correlated sampling in the specific prupose Monte Carlo codes McPNL and McDNL for simulating pulsed neutron and neutron porosity logging tools." *International journal of radiation applications and instrumentation. Part E, Nuclear geophysics*, 3(3), pp. 157-165.

Gardner, R. P., Prettyman, T. H., Mickael, M., and Verghese, K. (1988). "Some Geometric Modelling and Tracking Codes for Monte Carlo Particle Transport Including Direction Biasing Techniques." *Transactions of the American Nuclear Society*, 57, pp. 115-116.

Gillam, E., and Heal, H. T. (1952). "Some Problems in the Analysis of Steels by X-ray Fluorescence." *British Journal of Applied Physics*, 3, pp. 358.

Guo, W. (2002). "CEARXRF User's Guide." *Internal Usage*, North Carolina State University, Raleigh.

Guo, W., Gardner, R. P., and Metwally, W. A. (2003). "Preliminary Studies on K and L Coincidence Spectroscopy for Optimizing the *In Vivo* XRF Measurement of Lead in Bone." *Accepted by Nuclear Instruments and Methods B*, pp. TBD.

Hall, M. C. G. (1982). "Cross-section adjustment with Monte Carlo Sensitivities: application to the winfrith iron benchmark." *Nuclear Science and Engineering*, 81, pp. 423-431.

He, T. (1992). "Development of the Monte Carlo - Library Least-Squares Approach for Energy Dispersive X-Ray Fluorescence Analysis," Ph.D Thesis, NCSU, Raleigh.

He, T., Gardner, R. P., and Verghese, K. (1991). "NCSXRF: A general geometry Monte Carlo simulation for EDXRF analysis." *Advances in X-ray Analysis*, 35B, pp. 727-736.

He, T., Gardner, R. P., and Verghese, K. (1993). "The Monte-Carlo library least-squares approach for energy-dispersive X-ray fluorescence analysis." *Applied Radiation and Isotopes*, 44(10-11), pp. 1381-1388.

Herglotz, H., and Birks, L. S. (1978). *X-ray spectrometry*, M. Dekker, New York.

Hoogenboom, A. M. (1958). "A new method in gamma-ray spectroscopy: a two crystal scintillation spectrometer with improved resolution." *Nuclear Instruments*, 3, pp. 57-68.

Hubbell, J. H. (1975). "Atomic Form Factors, Incoherent Scattering Functions, and Photon Scattering Cross Sections." *Journal of physical and chemical reference data*, 4(3), pp. 471-538.

Jenkins, R. (1988). *X-ray fluorescence spectrometry*, J. Wiley, New York.

Jenkins, R., Gould, R. W., and Gedcke, D. (1981). *Quantitative x-ray spectrometry*, M. Dekker, New York.

Jenkins, R., Gould, R. W., and Gedcke, D. (1995). *Quantitative X-ray spectrometry*, M. Dekker, New York.

Jenkins, R., and Vries, J. L. d. (1970). *Practical X-ray spectrometry*, Springer-Verlag, New York.

Knoll, G. F. (2000). *Radiation detection and measurement*, Wiley, New York.

Kortright, J. B., and Thompson, A. C. (2002). "naming conventions for x-ray lines by showing the atomic shell structure."

Krause, M. O. (1979). "Atomic Radiative and Radiationless Yields for K and L shells." *Journal of physical and chemical reference data*, 8(2), pp. 307-327.

Lee, S. H. (1999). "Use of Differential Operators in the Monte Carlo - Library Least-Squares Method for X-ray Fluorescence Applications," Ph.D Thesis, NCSU, Raleigh.

Lee, S. H., Gardner, R. P., and Todd, A. C. (2001). "Preliminary studies on combining the K and L XRF methods for *in vivo* bone lead measurement." *Applied Radiation and Isotopes*, 54, pp. 893-904.

Lewis, D. G. (1994). "Optimization of a Polarized Source for *In Vivo* X-ray Fluorescence Analysis of Platinum and Other Heavy Metals." *Phys. Med. Biol.*, 34, pp. 197-206.

Lewis, D. G., Kilic, A., and Ogg, C. A. (1995). "Adaptation of the EGS4 Monte Carlo Code for the Design of a Polarized Source for X-ray Fluorescence Analysis of Platinum and Other Heavy Metals *In Vivo*." *Advances in X-ray Analysis*, 38, pp. 579-585.

Martin, R. H., and Taylor, J. G. V. (1992). "The standardization of ^{125}I: a comparison of three methods." *Nuclear Instruments and Methods in Physics Research A*, 312, pp. 64-66.

Nelson, W. R., Hirayama, H., and Rogers, D. W. O. (1985). "The EGS4 Code System." *SLAC-265*, Stanford Linear Accelerator Center.

NIM. (1990). *Standard NIM instrumentation system*, U.S. Dept. of Energy Office of Energy Research Office of Health and Environmental Research ;
Available from the National Technical Information Service, Washington, D.C.
Springfield, Va.

Ortec. (1999a). "Ge Detector Pulse Formation Process." http://www.ortec-online.com/detectors/review_physics/pulse.htm.

Ortec. (1999b). "Ortec Timing Discriminator User's Guide."

Pella, P. A., Feng, L., and Small, J. A. (1985). "An analytical algorithm for calculation of spectral distributions of X-ray tubes for quantitative X-ray fluorescence analysis." *X-ray Spectrometry*, 14, pp. 125-135.

Prettyman, T. H. (1992). "HERMETOR User's Guide." *Internal Usage*, North Carolina State University, Raleigh.

Prettyman, T. H., Gardner, R. P., and Verghese, K. (1990). "MCPT: A Monte Carlo Code for Simulation of Photon Transport in Tomographic Scanners." *Nuclear Instruments and Methods in Physics Research A*, 299, pp. 516-523.

Rief, H. (1984). "Generalized Monte Carlo Perturbation Algorithms for Correlated Sampling and a Second-order Taylor Series Approach." *Annals of nuclear energy*, 11(9), pp. 455-476.

Rief, H. (1994). "A Synopsis of Monte Carlo Perturbation Algorithms." *Journal of Computational Physics*, 111, pp. 33-48.

Rose, P. F. (1991). "ENDF/B-VI Summary Documentation." *ENDF-201*, National Nuclear Data Center, Upton, N.Y., U.S.A.

Scofield, J. H. (1974a). "Hartree-Fork Values of L X-Ray Emission Rates." *Physical Review A*, 10, pp. 1507-1510.

Scofield, J. H. (1974b). "Relativistic Hartree-Slater Values for K and L X-ray Emission rates." *Atomic Data and Nuclear Data Tables*, 14, pp. 121-137.

Shyu, C. M., Gardner, R. P., and Verghese, K. (1993). "Development of the Monte Carlo Library Least-Squares Method of Analysis for Neutron Capture Prompt Gamma ray Analyzers." *International journal of radiation applications and instrumentation. Part E, Nuclear geophysics*, 7(2), pp. 241-267.

Storm, E., and Israel, I. H. (1967). "Photon cross sections from 0.001 to 100 MeV for

elements 1 through 100." *Los Alamos Scientific Report LA-3753*, Los Alamos National Laboratory.

Tartari, A., Baraldi, C., Felsteiner, J., and Casnati, E. (1991). "Compton Scattering Profile for *In Vivo* XRF Techniques." *Phys. Med. Biol.*, 36, pp. 567-578.

Taylor, J. G. V. (1967). "x-ray-x-ray coincidence counting methods for the standardization of ^{125}I and ^{197}Hg, QC795 .S88 1966." Standardization of Radionuclides, IAEA, ed., Vienna, International Atomic Energy Agency, 1967., Vienna, 341.

Todd, A. C. (2000). "Coherent scattering and matrix correction in bone-lead measurements." *Phys. Med. Biol.*, 45(7), pp. 1953-1963.

Todd, A. C., McNeil, F. E., and Fowler, B. A. (1992). "*In Vivo* X-ray Fluorescence of Lead in Bone." *Environmental Research*, 59, pp. 326-335.

Verghese, K., Gardner, R. P., Mickael, M., Shyu, C. M., and He, T. (1988). "The Monte Carlo - Library Least-Squares Analysis Principle for Borehole Nuclear Well Logging Elemental Analyzers." *International journal of radiation applications and instrumentation. Part E, Nuclear geophysics*, 2(3), pp. 183-190.

Wallace, J. D. (1994). "The Monte Carlo Modelling of *In Vivo* X-ray Fluorescence Measurement of Lead in Tissue." *Phys. Med. Biol.*, 39, pp. 1745-1756.

Weber, M. J. (1998). *Selected papers on phosphors, light emitting diodes, and scintillators : applications of photoluminescence, cathodoluminescence, electroluminescence, and radioluminescence*, SPIE Optical Engineering Press, Bellingham, Wash. ;.

Williams, K. L. (1987). *An introduction to X-ray spectrometry : X-ray fluorescence and electron microprobe analysis*, Allen & Unwin, London ; Boston.